COLLISIONAL PROPERTIES OF BALL-RACKET INTERACTIONS IN TERMS OF NORMAL AND TANGENTIAL COEFFICIENTS OF RESTITUTION *

Suguru Araki[1], Shinichi Sato[2], and Hitoshi Yamazaki[2]
[1]Department of Physics, Hofstra University, Hempstead, NY 11550, USA
[2]Tokorozawa Laboratory, Tamasu Company Limited, Tokorozawa, Saitama 476, JAPAN

Submitted 04/04/96 to the International Journal of Table Tennis Sciences
Revised 06/24/96

KEY WORDS Collision dynamics, ball-racket interactions, hard-sphere models, normal and tangential coefficients of restitution.

ABSTRACT

Collision dynamics of the spinning table tennis balls are systematically studied by introducing a new parameter ϵ_t, the tangential coefficient of restitution, in addition to the conventionally accepted parameter ϵ_n, the normal coefficient of restitution. The normal coefficient of restitution describes the dissipative property of head-on collisions between the ball and the racket, which would be significant even if the spin degrees of freedom were completely ignored. The tangential coefficient of restitution is closely related to the surface properties of the two colliding members, and controls the coupling between translational and spin degrees of freedom. Among all the ball sports table tennis has the ball with the most extreme mass distribution: its total mass is concentrated within the outermost 2% region of the entire radius. Thus, the tangential coefficient of restitution plays a crucial role in the spin dynamics of table tennis.

In this paper we experimentally determine the dependence of the normal coefficient of restitution on the normal component of incident relative velocity. The tangential coefficient of restitution is also found to depend on the tangential component of incident relative velocity as well as on the incident angle. Making use of the simplest configuration of ball-racket collisions, we give the preliminary but first report of the dependence of the tangential coefficient of restitution upon incident speeds and angles. Most researchers in table tennis dynamics have treated the coefficients of restitution as constant parameters. Thus, the present work should help us evaluate to what extent these treatments are justified.

Further, taking the average of these coefficients over many collisions, we will be able to locate a variety of rackets, with and without glue effects, on the (ϵ_t, ϵ_n) diagram as a step toward classifying the commercially available rackets quantitatively on a physically sound basis.

---

* Based in part on a keynote speech given at the Fourth ITTF Sports Science Congress held in Beijing, the People's Republic of China, April 26–30, 1995.

1. INTRODUCTION

Collision dynamics of solid particles have been a subject of extensive studies in many fields of science and engineering. In astronomy planetary rings such as Saturn's classical rings are considered large-scale grain flow phenomena in which shear flows of many chunks of icy rock undergo inelastic collisions while orbiting a central planet. Similar granular flows of a smaller scale are common in a geophysical context, including snow avalanches, landslides, sand dunes, and volcanic ejecta flows. In engineering numerous applications exist in materials transport and handling which involve rapid shear flows, from fine powder to large grains. Understanding the behavior of these granular flows is also important in the pharmaceutical and mineral industries in relation to their size sorting and transport problems (e.g. Savage and Sayed 1984).

In this paper we apply the mathematical machinery developed for theoretical studies of dissipative collisions between icy particles in planetary rings [Araki and Tremaine (1986), Araki (1988, 1991a, 1991b)] to the collisional interactions between table tennis balls and rackets as an attempt to provide our sport with a physically rigorous basis.

We make a major assumption at the outset: We assume that the table tennis ball is a "hard" sphere, that is, undeformable under the influence of collisional impulse. We also assume that the racket has an undeformable flat surface. If both the ball and the racket are assumed hard, then their collisional interaction can be well approximated as that of two hard spheres with one member having much greater radius and mass than another. Of course, any active player would certainly reject this assumption since deformations of the ball and the racket surface are significant even in moderately high-speed collisions. Moreover, we all know that understanding and enhancement of elastic deformation of colliding members, especially that of the blade complex including the top rubber sheet, the sponge, and the blade, is the latest issue in modern table tennis among players and manufacturers alike. Therefore, we must keep a careful eye on when the assumption of hard-sphere collisions breaks down. Due to its geometrical simplicity, however, even a hard-sphere model can tell us much about the ball-racket interaction as we show in the following sections.

Under the above assumption the details of complex ball-racket interactions during a collision can be reduced to two simple parameters, ϵ_n and ϵ_t, which in the present work we call the normal and tangential coefficients of restitution. Each coefficient is a factor by which a certain component of the incident relative velocity between points of contact is altered due to a collision. Although it is customary to assume that to a first approximation these coefficients are constant and independent of the magnitude and direction of the incident relative velocity, it is known that in real collisions ϵ_n and ϵ_t may depend substantially on the incident relative velocity.

In the context of collision dynamics of planetary rings experimental studies on the velocity dependence of the above coefficients have been actively pursued over the last decade. Bridges *et al.* (1984) were the first to attempt to determine the velocity dependence of the normal coefficient of restitution during head-on collisions of ice balls against a stationary ice brick at low ambient temperatures at Saturn. They found a power-law dependence $\epsilon_n = \alpha v_n^{-\beta}$ with $\alpha = 0.32$ and $\beta = 0.234$ at $T = 158$ to 173 K when the incident normal speed v_n was measured in cm/s. Later Hatzes *et al.* (1988) concluded that

changing the surface property from smooth to frost-covered and rough significantly reduced the elasticity of normal collisions. Hatzes *et al.* (1991) measured the sticking force in the presence of a layer of water frost 10 to 100 μm thick on the surfaces of colliding ice spheres, and found a maximum for some intermediate impact velocity between 0.01 and 1 cm/s. Supulver *et al.* (1995) were the first to experiment on glancing collisions of ice spheres with unfrosted surfaces using a combination of a disk pendulum and a torsion pendulum. The disk pendulum alone with fixed torsion pendulum simulates normal collisions while the torsion pendulum provides colliding members with an additional degree of freedom within the plane tangent to the colliding surfaces. Restricting to the normal collisions, they first reproduced the power-law dependence $\epsilon_n(v_n)$ with $\alpha = 0.51$ and $\beta = 0.19$ for fixed torsion pendulum, while $\alpha = 0.52$ and $\beta = 0.14$ for free torsion pendulum (FIG. 3 in Supulver *et al.* 1995). For glancing collisions of smooth ice particles, they found the following linear least-square fits: $\epsilon_n = 0.59 - 0.11 v_n$ at $v_n > 0.1$ cm/s, and $\epsilon_t = 0.88 - 0.0038 v_t$ at $v_t > 0.1$ cm/s. At impact speeds lower than 0.1 cm/s the scatter of data was significant, probably because the surface irregularities had the largest effect at those speeds (FIG. 5 in Supulver *et al.* 1995). An additional experiment on glancing collisions of a rubber ball against a flat sandpaper-covered aluminum plate (FIG. 10 in Supulver *et al.* 1995) showed that while ϵ_n was rather constant over a range of impact angles, ϵ_t clearly depended on the impact angle.

In the context of ball-racket collisions in table tennis Tiefenbacher and Durey (1994a, 1994b) were the first to propose the usefulness of tangential coefficient of restitution, while others including Kawazoe (1992) have focused on the conventional coefficient of restitution in head-on collisions of spinless balls with rackets.

In this paper we attempt to examine the validity of hard-sphere collision models based on ϵ_n and ϵ_t in table tennis dynamics. We also experimentally determine the dependence of ϵ_t on the incident relative speed, incident angle, and ϵ_n.

2. BASIC EQUATIONS OF COLLISION DYNAMICS

We consider a collision of two hard spheres in a three dimensional space and formulate the laws of momentum conservation and of angular momentum conservation in the impulse approximation. A hard sphere is characterized by its radius, mass, and moment of inertia. For an ITTF-approved table tennis ball its radius is $r = 1.9$ cm, mass is $m = 2.5$ g, and moment of inertia is

$$I = \frac{2}{5}\frac{1-(1-t/r)^5}{1-(1-t/r)^3} mr^2 = 0.653 mr^2 = 5.89 \mathrm{gcm}^2,$$

assuming that the ball is a spherical shell of thickness $t = 0.04$ cm. Suppose Particle 1 with radius r_1, mass m_1, moment of inertia I_1, incident velocity $\vec{v}_1$, and incident angular velocity $\vec{\omega}_1$ collides with Particle 2 with radius r_2, mass m_2, moment of inertia I_2, incident velocity $\vec{v}_2$, and incident angular velocity $\vec{\omega}_2$ (Figure 1). The corresponding postcollision velocities and angular velocities are primed. If the position vectors of spherical centers of the colliding members in contact are $\vec{x}_1$ and $\vec{x}_2$, the collision site is given by $\vec{x}_1 + r_1\vec{\lambda}$ where

$$\vec{\lambda} = \frac{\vec{x}_2 - \vec{x}_1}{r_1 + r_2} \tag{1}$$

is a unit vector on a straight line connecting two centers which defines the "collision normal." The plane perpendicular to the collision normal and containing the collision site is the "collision tangent." Then, the conservation of momentum requires

$$m_1(\vec{v}_1' - \vec{v}_1) = -\Delta\vec{P} \tag{2}$$

$$m_2(\vec{v}_2' - \vec{v}_2) = \Delta\vec{P} \tag{3}$$

where $\Delta\vec{P}$ is the impulse exerted on Particle 2 by Particle 1. The conservation of angular momentum leads to

$$I_1(\vec{\omega}_1' - \vec{\omega}_1) = r_1\vec{\lambda} \times (-\Delta\vec{P}) \tag{4}$$

$$I_2(\vec{\omega}_2' - \vec{\omega}_2) = r_2(-\vec{\lambda}) \times \Delta\vec{P} \tag{5}$$

3. NORMAL AND TANGENTIAL COEFFICIENTS OF RESTITUTION

In this section we give the mathematical definition of the normal and tangential coefficients of restitution which together describe the dissipative character of hard-sphere collisions. We first define the precollision relative velocity of the center C_1 of Particle 1 with respect to the center C_2 of Particle 2 and its postcollision counterpart

$$\vec{g} = \vec{v}_1 - \vec{v}_2 \tag{6}$$

$$\vec{g}' = \vec{v}_1' - \vec{v}_2'. \tag{7}$$

Then, we define the precollision relative velocity of the point of contact P_1 on the surface of Particle 1 with respect to the point of contact P_2 on the surface of Particle 2 and its postcollision counterpart

$$\vec{W} = \vec{g} + (r_1\vec{\omega}_1 + r_2\vec{\omega}_2) \times \vec{\lambda} \tag{8}$$

$$\vec{W}' = \vec{g}' + (r_1\vec{\omega}_1' + r_2\vec{\omega}_2') \times \vec{\lambda} \tag{9}$$

Decomposition of $\vec{W}$ into the normal and tangential directions yields

$$\vec{W}_n \equiv (\vec{\lambda} \cdot \vec{W})\vec{\lambda} = \vec{g}_n \tag{10}$$

$$\vec{W}_t \equiv \vec{W} - \vec{W}_n = (\vec{\lambda} \times \vec{W}) \times \vec{\lambda} = \vec{g}_t + (r_1\vec{\omega}_1 + r_2\vec{\omega}_2) \times \vec{\lambda} \tag{11}$$

With the above introduced velocities we define the normal coefficient of restitution as a factor by which the normal component W_n of the relative velocity of two surface points coming into contact is altered due to a collision:

$$\vec{W}_n' = -\epsilon_n\vec{W}_n \qquad (0 \le \epsilon_n \le 1) \tag{12}$$

Similarly, the tangential coefficient of restitution is defined as a factor by which the tangential component W_t is altered due to the collision:

$$\vec{W}_t' = \epsilon_t\vec{W}_t \qquad (-1 \le \epsilon_t \le 1) \tag{13}$$

The normal coefficient of restitution is identical with the conventional coefficient of restitution and has nonnegative values. However, the tangential coefficient of restitution introduced in Eq. (13) can range between -1 and $+1$ and positive values represent the surface roughness while negative values correspond to the tangential elasticity, as described in more detail at the end of Section 4.

Our objective is to examine how the choice of characteristics of colliding memebers affects the values of these coefficients, and also whether they remain constant over a variety of incident relative velocities. If they do not remain constant, we study what they depend upon, specifically the W_n dependence of ϵ_n, the W_t dependence of ϵ_t, and the possible relation between ϵ_t and ϵ_n.

4. SOLUTION IN 3D

With the above preparation we will find the solution of hard-sphere collisions in three dimensions. Combining Eqs. (2), (3), (4), (5), (8), and (9), we can now express the normal and tangential components of impulse on Particle 2 exerted by Particle 1 in terms of precollision variables:

$$\Delta\vec{P}_n = 2\mu\kappa_n\vec{W}_n \tag{14}$$

$$\Delta\vec{P}_t = 2\mu\kappa_t\vec{W}_t, \tag{15}$$

where

$$\kappa_n \equiv \frac{1+\epsilon_n}{2} \tag{16}$$

$$\kappa_t \equiv \frac{1-\epsilon_t}{2}\left[1+\mu\left(\frac{r_1^2}{I_1}+\frac{r_2^2}{I_2}\right)\right]^{-1} \tag{17}$$

and

$$\mu \equiv \frac{m_1 m_2}{m_1+m_2} \tag{18}$$

is the reduced mass. Then, we can solve for the postcollision velocities and angular velocities:

$$\vec{v}_1' = \vec{v}_1 - \frac{2\mu}{m_1}(\kappa_n\vec{W}_n + \kappa_t\vec{W}_t), \tag{19}$$

$$\vec{v}_2' = \vec{v}_2 + \frac{2\mu}{m_2}(\kappa_n\vec{W}_n + \kappa_t\vec{W}_t) \tag{20}$$

$$\vec{\omega}_1' = \vec{\omega}_1 - \frac{2\mu\kappa_t r_1}{I_1}\vec{\lambda}\times\vec{W}, \tag{21}$$

$$\vec{\omega}_2' = \vec{\omega}_2 - \frac{2\mu\kappa_t r_2}{I_2}\vec{\lambda}\times\vec{W} \tag{22}$$

From Eqs. (21) and (22) we find that when $\kappa_t = 0$ angular velocities are unaffected by collisions. In other words spin and translational degrees of freedom are totally decoupled when $\kappa_t = 0$. In this sense κ_t can be considered as the coupling constant between the two degrees of freedom. The definition Eq. (17) shows that $\kappa_t = 0$ is equivalent to either

$\epsilon_t = 1$ or $I_1 = 0$ or $I_2 = 0$. First, as mentioned below, $\epsilon_t = 1$ corresponds to the property of perfectly slippery surfaces. Obviously, in this case spin on the ball would not affect the fate of its translational motion. Second, if one of the colliding members has such a radial mass distribution that all the mass is concentrated at its center, the decoupling is perfect. This is a rather unphysical situation, but for the sport of table tennis it is especially significant to consider the opposite extreme. That is, among all the ball sports the table tennis ball has the most extreme mass distribution: its total mass is concentrated within the outermost 2% region of the entire radius. Thus, the dimensionless moment of inertia of a table tennis ball $I^* = I/mr^2 = 0.653$ almost carries its maximum value 2/3, giving it almost the strongest coupling between spin and translational degrees of freedom (Figure 2). We believe that this is the single crucial factor which distinguishes table tennis from the rest of the sports. Table tennis is the sport of the greatest spin-translation coupling constant in which most frequent and severe excitation of spin degrees of freedom can be achieved.

Once we have found the solution, it is possible to obtain various quantities of physical interest. Among others, the change in translational kinetic energy of two colliding members due to the collision is

$$\Delta E^{(T)} = \frac{1}{2}(m_1 v_1'^2 + m_2 v_2'^2 - m_1 v_1^2 - m_2 v_2^2) = -\mu\kappa_n(1-\epsilon_n)W_n^2 - X \tag{23}$$

and the change in spin kinetic energy of these particles is

$$\Delta E^{(S)} = \frac{1}{2}(I_1\omega_1'^2 + I_2\omega_2'^2 - I_1\omega_1^2 - I_2\omega_2^2) = -\mu\kappa_t(1+\epsilon_t)W_t^2 + X \tag{24}$$

where

$$X \equiv 2\mu\kappa_t(\vec{g}_t - \kappa_t\vec{W}_t)\cdot\vec{W}_t \tag{25}$$

represents the flow of kinetic energy from translational to spin degrees of freedom as a result of this collision. Finally, the change in total kinetic energy is given by

$$\Delta E = \Delta E^{(T)} + \Delta E^{(T)} = -\mu[\kappa_n(1-\epsilon_n)W_n^2 + \kappa_t(1+\epsilon_t)W_t^2]. \tag{26}$$

Let us consider the significance of the coefficients of restitution in terms of energy dissipation. In Eq. (23) the change in translational kinetic energy consists of energy loss due to inelasticity of collisions and outflow into spin degrees of freedom. Since κ_n contains a factor $1-\epsilon_n$ [Eq. (16)] and thus the dissipative loss is proportional to $1-\epsilon_n^2$, we see that, as far as the normal direction is concerned, $\epsilon_n = 1$ corresponds to the perfectly elastic collision while $\epsilon_n = 0$ corresponds to the perfectly inelastic collision (Figure 3).

Next, Eq. (24) together with Eq. (17) shows that the change in spin energy due to a collision is a balance between the energy loss proportional to $1-\epsilon_t^2$ and the energy inflow from the translational degrees of freedom X. When $\epsilon_t = 1$, the tangential component of the relative veocity between the two points coming into contact is unchanged immediately after collision. This is the case of perfectly slippery surfaces. In this case spin degrees of freedom can be totally neglected since they are decoupled from translational degrees of freedom. That is, spin does not affect the course of dynamical evolution of translational motion.

Surface properties represented by positive ϵ_t correspond to various degrees of roughness. However, the tangential component of the postcollision relative velocity maintains the same direction as that of the precollision relative velocity. A perfectly rough surface is represented by $\epsilon_t = 0$ since the tangential component of the relative velocity between two surface points coming into contact vanishes immediately after the collision. Most long pips rubber, hard rubber, antispin rubber, and natural wood surfaces including official table surfaces would belong to the positive ϵ_t category, though their degrees of normal elasticity may vary significantly.

However, ϵ_t can systematically classify another kind of surface property at its negative values. In some collisions such as those of table tennis balls on sticky inverted rubber the tangential component of the relative velocity reverses its direction. A part of the incident spin as well as translational kinetic energy is first converted into elastic energy in strained colliding members gripping each other, and subsequently this strain energy is reconverted into the spin and translational kinetic energy of the outgoing particles. We will call this property as the "tangential elasticity." At $\epsilon_t = 0$ there is no tangential elasticity, and since the colliding members grip each other, it is equivalent to a perfectly rough surface. As $|\epsilon_t|$ increases, the tangential elasticity also increases, and reaches its maximum at $\epsilon_t = -1$ where no energy is lost as far as the sum of kinetic energies associated with the linear motion in the tangential direction and spin are concerned. Most dissipative surfaces are characterized by $(\epsilon_n,\ \epsilon_t)=(0,\ 0)$ while energy is conserved at collisions when $(\epsilon_n,\ \epsilon_t)=(1,\ 1)$ or $(\epsilon_n,\ \epsilon_t)=(1,\ -1)$. Manufacturers of spinniest modern inverted rubbersheets make every effort to increase their tangential elasticity while keeping their normal elasticity substantial. Short pips soft rubbersheets seem to maintain high normal elasticity while their tangential elasticity is held relatively low. Estimates of representative values of the normal and tangential coeficients of restitution of table tennis rubber manufactured by Tamasu in the recent decade are given in Figure 3. Since in reality these coefficients are velocity-dependent, the values shown in this figure should be considered as the average over many collisions at a variety of incident relative velocities.

5. 2D MODELS WITH DISPARATE MASS RATIO

Up to Section 4. we have been discussing the general case of collisions between hard spheres. Having a particular application of the above formulation to model experiments in table tennis in mind, we now restrict ourselves to the two-dimensional models with a disparate mass ratio.

In considering collisions between a racket and a ball, we know that an official table tennis ball has the standard mass of 2.5 g while a typical player with a racket weighs at least 60 kg. In collisions between the balls and the tables colliding members are even heavier, exceeding 100 kg. In these cases a typical mass ratio is as small as $m_1/m_2 \sim O(10^{-5})$, the reduced mass is $\mu \sim m_1$, and thus practically Particle 2 can be considered stationary. Hereafter, we focus on the motion of Particle 1 in a collision with a stationary partner Particle 2, and omit the suffixes of Particle 1.

The restriction to 2D models is imposed simply for experimental convenience. We first require that the incident velocity has no z-component: $\vec{v}_1 = (u, -v, 0)$. We further assume

that the incident ball has no side-spin, or more exactly, that its precollision spin has only a z-component: $\vec{\omega}_1 = (0, 0, \omega)$ (Figure 4). Then, it is guaranteed that the postcollision spin also has only a z-component.

Under the above conditions the laws of momentum conservation and of angular momentum conservation given in the previous section are reduced to the following forms:

$$v' = \epsilon_n v \tag{27}$$

$$u' + r\omega' = \epsilon_t(u + r\omega) \tag{28}$$

$$m(u' - u) = -\Delta P_t \tag{29}$$

$$m(v' + v) = \Delta P_n \tag{30}$$

$$I(\omega' - \omega) = -r\Delta P_t \tag{31}$$

from which the 2D solutions are found:

$$v' = \epsilon_n v$$

$$u' = (1 - 2\kappa_t)u - 2\kappa_t \omega r$$

$$\omega' = -\frac{2\kappa_t}{I^*}\frac{u}{r} + \left(1 - \frac{2\kappa_t}{I^*}\right)\omega$$

$$\Delta P_n = 2\kappa_n m v, \qquad \kappa_n = \frac{1 + \epsilon_n}{2}$$

$$\Delta P_t = 2\kappa_t m(u + r\omega), \quad \kappa_t = \frac{1 - \epsilon_t}{2}\frac{I^*}{I^* + 1}$$

where the dimensionless moment of inertia of Particle 1 is $I^* = I/(mr^2) = 0.653$, appropriate for the official table tennis ball.

6. MODEL EXPERIMENTS

A series of 2D collision experiments with the two simplest configurations were performed at Tamasu's Tokorozawa Laboratory. One with falling balls with finite initial spin, "Model I," and another with nonrotating balls with some angle of incidence, "Model II." In both Models a stationary racket surface lies in the horizontal plane x-z, and the collision events take place within the vertical plane x-y (Figure 4).

(i) Model I: $u = 0$

In Model I a table tennis ball is given a clockwise initial spin $\omega < 0$ and is released vertically downward at an initial velocity $(0, -v)$ in the vicinity of the racket surface. The gravitational force on the ball can be neglected compared with the impulsive force exerted during the collision so long as a typical linear speed v substantially exceeds $g\Delta t \sim 1$ cm/s. Here $\Delta t \sim 1$ ms is a typical duration of collision, and $g = 980$ cm/s^2 is the gravitational

acceleration. After the collision with the racket surface the ball is deflected toward the positive x direction. The postcollision velocity (u', v') and spin ω' are

$$v' = \epsilon_n v, \quad \Delta P_n = (1+\epsilon_n)mv, \quad \Delta P_t = \frac{I^*}{1+I^*}(1-\epsilon_t)mr\omega$$

$$u' = \frac{I^*}{I^*+1}(1-\epsilon_t)r(-\omega) \tag{a}$$

$$-\omega' = \frac{I^*+\epsilon_t}{I^*+1}(-\omega) \tag{b}$$

$$\epsilon_t = 1 - \frac{I^*+1}{I^*}\frac{u'}{r(-\omega)} \tag{a'}$$

$$\epsilon_t = (I^*+1)\frac{-\omega'}{-\omega} - I^* \tag{b'}$$

(ii) Model II: $\omega = 0$

In the Model II experiment a ball without initial spin and with an initial velocity $(u, -v)$ is incident upon the racket surface. After the collision the ball acquires the spin ω' as well as the velocity (u', v') which are given by

$$v' = \epsilon_n v, \quad \Delta P_n = (1+\epsilon_n)mv, \quad \Delta P_t = \frac{I^*}{1+I^*}(1-\epsilon_t)mu$$

$$u' = \frac{1+I^*\epsilon_t}{1+I^*}u \tag{c}$$

$$-\omega' = \frac{1-\epsilon_t}{1+I^*}\frac{u}{r} \tag{d}$$

$$\epsilon_t = \frac{1+I^*}{I^*}\frac{u'}{u} - \frac{1}{I^*} \tag{c'}$$

$$\epsilon_t = 1 - (1+I^*)\frac{r(-\omega')}{u} \tag{d'}$$

Before we report our experimental results we briefly describe the characteristics of the apparatus used in these experiments. Our experimental apparatus mainly consists of a high speed video recorder and a ball machine in addition to the balls and the racket mount.

Top international players are known to produce the ball speed of up to 120 km/h immediately after the impact in typical smashing strokes. The maximum top spin loaded on the ball by top international players reaches 150 rps (Wu *et al.* 1992). The present ball machine has the capability to reproduce the above maximum speed and spin. This ball machine has a pair of parallel-axis rotors with high friction rubber surfaces. The diameter of each rotor is 13 cm, and the gap between the rotors is slightly narrower than the ball diameter 3.8 cm. The maximum spin of $n \sim 12000$ rpm ~ 200 rps and the maximum speed of $v \sim 3000$ cm/s ~ 100 km/h can be generated by this ball machine.

Another major component of our experimental apparatus is a high speed video recorder, Kodak Ektapro HS Motion Analyzer HS4540. It can take images of fast-moving balls at the highest frequency of 40500 pps (pictures per second). A maximum of 81920 images can be recorded and stored in IC memory chips. The replay, fast forwarding, rewinding, and pause of recorded images can be performed quite easily just as one uses a commercial video tape recorder. In the present experiments all the pictures were taken at 4500 pps, considering the dimension of the imaging space and the effects of errors in measurements. A set of movable x-y cordinate axes can be placed on the monitor screen during the replay of recorded images. By translating this coordinate system over the images we can analyze the motion of the balls quite efficiently. The minimum displacement of the coordinate system in x or y directions is limited by the size of a single pixel of the monitor screen. The entire frame is covered with 256×256 pixels.

Finally, we briefly describe the actual procedures we have followed to determine the speed and spin of the ball from its images. The ball speed is determined by dividing its displacement $\Delta r = \sqrt{(\Delta x)^2 + (\Delta y)^2}$ by the corresponding time interval Δt. As mentioned above most images were taken at 4500 pps, and thus the time resolution of the ball behavior is 1/4500 seconds. Practically, however, most measurements of the displacement were done every ten pictures [$\Delta t = 1/4500(s/p) \times 10(p) = 1/450$ s] without loss of accuracy. Since the raw displacement is read off from the screen images, its conversion into the true displacement must be done. In order to establish this scale conversion, the number of pixels over the diameter of slowly moving balls was counted: 110 pixels in 3.8 cm. Thus, 1 pixel corresponds to the actual length $s = 0.0345$ cm/pixel. If a certain displacement of the ball during a 10-picture time interval occurs over N_x pixels along the x axis, the x component of the speed is thus found by

$$v_x(\mathrm{cm/s}) = \frac{N_x(\mathrm{pixel}) \times s(\mathrm{cm/pixel})}{\Delta t(\mathrm{s})}.$$

Together with the measurement of N_y to obtaine the y component v_y, we can determine the two-dimensional speed of the ball.

The magnitude of the ball spin is the number of rotations per unit time. In the current experiments we have printed alphabetic letters uniformly over the ball surface so that the spin can be read off from arbitrary viewing directions. The number of rotations n (r/s) was found by counting the number of pictures N_s over which a particular alphabetic letter on the ball surface rotated through a certain angle θ (deg):

$$n(\mathrm{r/s}) = \frac{4500(\mathrm{p/s})}{N_s \times 360°/\theta°(\mathrm{p/r})}.$$

Note that in this paper n (r/s) and the angular speed ω (rad/s) are interchangeably used to describe the spin on table tennis balls, but they are related to one another by $\omega = 2\pi n$ since one rotation corresponds to 2π radians.

7. RESULTS

(i) Velocity Dependence of ϵ_n

We begin with the investigation of the velocity dependence of ϵ_n. Table tennis balls with no initial spin $\omega = 0$ and with vertically downward initial speed $(0, -v)$ are incident on a Butterfly basic red Sriver rubbersheet with 1.9-mm thick sponge fixed on a 50-mm thick horizontal woodblock with PSA (pressure sensitive adhesive). Here "basic" means that it is not a Sriver FX, and "red" since a possibility cannot be totally excluded that color might introduce the variation in rubber properties. We vary the incident speed v from 20 to 100 km/hr, and calculate the coefficient of normal restitution using $\epsilon_n = v'/v$. The result is shown in Figure 5. Obviously ϵ_n is not constant but dependent on v. It is found that ϵ_n is smaller at higher v, that is, collisions at higher impact speeds are more dissipative. It is also observed that $d\epsilon_n/dv \to 0$ at high v: At higher impact speeds the constant-ϵ_n approximation becomes progressively better. Specifically, in this experiment $\epsilon_n \to\sim 0.4$ at high $v > 100$ km/hr. In another extreme $\epsilon_n \sim 1$ at low impact speeds. The power-law best fit for 22 collisions is

$$\epsilon_n = 9.86 \times v(\mathrm{cm/s})^{-0.392}$$

which attains the maximum value $\epsilon_n = 1$ at $v = 344$ cm/s. Thus, at incident speeds less than 344 cm/s or 12.4 km/h all the normal collisions against the present Sriver racket surface are perfectly elastic and nondissipative. Combined with the experiments in the following subsections, it is also found that the above velocity dependence $\epsilon_n(v)$ is unaffected by the existence of finite relative velocity in the tangential direction $W_t = u + r\omega$, though the scatter in the data points becomes more significant.

Incidentally, the ITTF Laws of Table Tennis state that the table surface may be of any material and shall yield a uniform bounce of about 23 cm when a standard ball is dropped on to it from a height of 30 cm (e.g. ITTF 1995). This condition requires the normal coefficient of restitution $\epsilon_n = 0.876$ at the incident speed $v = 242$ cm/s $= 8.73$ km/h for a typical ball-table collision of low impact.

(ii) Velocity Dependence of ϵ_t

In this subsection we report a series of four experiments related to one another: [1] Model I experiment on Sriver glued with PSA, [2] Model II experiment on Sriver glued with PSA, [3] Model I experiment on Feint glued with PSA, [4] Model I experiment on Sriver glued with trichloroethylene and with Butterfly Clean Chack.

[1] Model I experiment on Sriver glued with PSA In this experiment table tennis balls at given vertical speeds v with a variety of initial spin n are normally (in the y direction) incident on a Sriver rubbersheet attached to a horizontal surface (x-z plane) of a woodblock with PSA. Thus, balls have no tangential component in initial velocity: $u = 0$. The spin axis of the balls is oriented in the z direction so that the postcollision spin also has only the z component n'. We restrict ourselves only to two incident speeds, 30 km/h and 70 km/h, but in each case we vary the initial spin from 0 rps up to 200 rps, and measure the postcollision velocity (u', v') and spin n'. The results are shown in Figure 6. In the case of $v = 70$ km/h we have plotted (n, u') in Figure 6a, and (n, n') in Figure 6b.

According to Eqs. (a) and (b), if ϵ_t were a pure constant over many collisions, these plots should be best fit with a straight line passing through the origin. Imposing a linear

fit with vanishing intercepts on these plots, we find the best-fit slope $m_1 = 5.5259$ and the corresponding $\epsilon_t(a') = 1 - [1 + (1/I^*)][m_1/(2\pi r)] = -0.172$ from Figure 6a, and $m_1 = 0.16026$ and $\epsilon_t(b') = (1 + I^*)m_1 - I^* = -0.388$ from Figure 6b. The discrepancy between the two values of ϵ_t obtained from the above two linear fits is mainly ascribed to the deformation of colliding members which is never taken into account in the hard-sphere collision models. In fact we observe significantly less discrepancy in the $v = 30$ km/h case where the collisional deformation is expected to be smaller. In the latter case the best linear fits passing through the origin yield $m_1 = 7.052$ and $\epsilon_t(a') = -0.496$ from Figure 6c, and $m_1 = 0.053682$ and $\epsilon_t(b') = -0.564$ from Figure 6d. Obviously, the hard-sphere models are expected to describe low impact collisions reasonably well while the detailed description of collisional deformation becomes crucial at high impact collisions.

However, even at moderately low impact collisions Figure 6 shows that the assumption of constant ϵ_t may be poor. In fact, one of the authors, H. Yamazaki, found that at very low spin the direction of spin is reversed as a result of collisions, giving ϵ_t a value lower than $-I^* = -0.653$. This phenomenon cannot be explained so long as we ignore the velocity dependence of ϵ_t. When n is not very large, rubber will decelerate the spin on the ball within a duration of contact (~ 0.9 ms at $v = 70$ km/h) to the extent that the postcollision spin becomes reversed. However, if n is sufficiently large, the ball will leave the contact site before the incident spin is substantially altered within a duration of contact. Further, we know that high speed collisions have longer contact durations and are less elastic. If there is a positive correlation between ϵ_n and ϵ_t in the ball-racket interaction, the tendency to suppress and reverse the initial spin would be less significant, and consequently there would be a smaller interval of reversed postcollision spin in the (n, n') diagram. On the contrary, low impact collisions have shorter contact durations and are more elastic. Again, if we assume a positive correlation between the two coefficients of restitution, we would conclude that the tangential elasticity in low impact collisions is relatively higher, and spin reversal trend would be more pronounced, resulting in a greater interval of reversed outgoing spin. The above situation can be viewed more quantitatively if we choose to apply the linear fitting to the (n, ϵ_t) plot in Figure 7:

$$\epsilon_t = A_1 + B_1 n. \tag{32}$$

Once we obtain the linear regression coefficients A_1 and B_1, we insert Eq. (32) into Eqs. (a) and (b) to find the following quadratic approximations:

$$u' = -C_a n(n - n_a) \quad \text{where} \quad C_a = \frac{2\pi r B_1 I^*}{1 + I^*} \quad \text{and} \quad n_a = \frac{1 - A_1}{B_1} \tag{33}$$

$$n' = C_b n(n - n_b) \quad \text{where} \quad C_b = \frac{B_1}{1 + I^*} \quad \text{and} \quad n_b = -\frac{I^* + A_1}{B_1}. \tag{34}$$

Since in Figure 7a the data set (n, ϵ_t) obtained with the use of Eq. (b') shows the better fitness R than that obtained with the use of Eq. (a'), we adopt $A_1 = -0.80064$ and $B_1 = 0.0029168$. Then, we find $C_a = 0.0138$, $n_a = 617$, $C_b = 0.00177$, and $n_b = 50.7$. Therefore, the best estimate of the maximum initial spin which produces the reversed final spin is 50.7 rps at $v = 70$ km/h. Similar calculations show that at $v = 30$ km/h

$A_1 = -0.81956$ and $B_1 = 0.0019609$ yield $C_a = 0.00925$, $n_a = 928$, $C_b = 0.00119$, and $n_b = 85.0$ (Figure 7b). Thus, the interval of initial spin n which causes the reversed final spin n' is broader at $v = 30$ km/h as argued above (Figure 6b and 6d).

Finally, we find in Figure 7 that the scatter in the (n, ϵ_t) data is significantly more pronounced at higher incident speed v and at lower initial spin n. Also, the discrepancy between the data set (n, ϵ_t) obtained from Eq. (a') and that obtained from Eq. (b') becomes more significant at higher incident speed v and at lower initial spin n. This is probably because higher v and less n allow the ball to deform more severely at collisions. Greater spin is expected to prevent the ball from larger deformation so that the hard-sphere approximation becomes a good one in higher spin regime.

[2] Model II experiment on Sriver glued with PSA Model II collision experiments are performed also within the x-y plane. Incident balls have initial velocity (u, $-v$) but have no initial spin: $\omega = 0$. The incident angle $\theta = \arctan(v/u)$ is defined relative to the racket surface lying in the x-z plane. The final velocity has no $\hat{z}$ comonent (u', v', 0) while the final spin has only the z component (0, 0, ω'). For practical reasons, we again restricted ourselves to two initial normal speeds, $v = 30$ km/h and 50 km/h, and recorded the final velocities and spin for a variety of initial tangential speeds u ranging from 0 up to 2500 cm/s. The results are shown in Figure 8.

Assuming that ϵ_t is velocity independent, the best linear fit passing through the origin to the (u, n') data at $v = 50$ km/s (Figure 8b) has a slope $m_1 = 0.072881$ which yields the best estimate for $\epsilon(d') = 1 - 2\pi r(1 + I^*)m_1 = -0.438$ while the similar analysis of the (u, u') data at $v = 50$ km/h leads to $m_1 = 0.40582$ which yields $\epsilon_t(c') = [m_1(1 + I^*) - 1]/I^* = -0.504$ (Figure 8a). A repeated linear regression analysis at $v = 30$ km/h shows a slope $m_1 = 0.080427$ and a estimate $\epsilon_t(d') = -0.587$ from Figure 8d, and $m_1 = 0.38444$ and a estimate $\epsilon_t(c') = -0.558$ from Figure 8c. If the hard-sphere approximation were to hold perfectly, the discrepancy between $\epsilon_t(c')$ and $\epsilon_t(d')$ should disappear since the (u, u') data and the (u, n') data are generated from the same collision events. Therefore, it is reasonable to argue that the lower the normal incident speed v, the less the collisional deformation of the ball and racket and consequently the less the discrepancy between the two data sets. We also find that the magnitude of ϵ_t increases as v decreases, which indicates that there is a positive correlation between the tangential elasticity and the normal elasticity.

However, the (u, ϵ_t) plots in Figure 9 shows a clear indication that the constant-ϵ_t approximation must be reconsidered. At least the tangential elasticity $-\epsilon_t$ is more pronounced at lower tangential speeds u. To seek a better approximation, we apply the linear regression analysis to the (u, ϵ_t) data sets:

$$\epsilon_t = A_2 + B_2 u. \tag{35}$$

Once we obtain the above coefficients, we insert Eq. (35) into Eqs. (c) and (d) to find the following quadratic approximations:

$$u' = C_c u(u - u_c) \quad \text{where} \quad C_c = \frac{B_2 I^*}{1 + I^*} \quad \text{and} \quad u_c = -\frac{1 + I^* A_2}{I^* B_2} \tag{36}$$

$$n' = -C_d u(u - u_d) \quad \text{where} \quad C_d = \frac{B_2}{2\pi r(1 + I^*)} \quad \text{and} \quad u_d = \frac{1 - A_2}{B_2}. \tag{37}$$

Since the best linear fit of ϵ_t resulting from Eq. (c') goes below -1 at low tangential speeds u, we choose to retain only the results from $\epsilon_t(d')$ plots. In Figure 9a we find the best estimate of the velocity dependence at $v = 50$ km/h to be $\epsilon_t = A_2 + B_2 u$ with $A_2 = -0.70396$ and $B_2 = 0.00012921$, which leads to $C_c = 0.0000510$, $u_c = -6410$, $C_d = 0.0000655$, and $u_d = 13200$. Similarly, the linear fitting of $(u, \epsilon_t(d'))$ data at $v = 30$ km/h in Figure 9b yields $A_2 = -0.86279$, $B_2 = 0.00016088$, which leads to $C_c = 0.0000635$, $u_c = -4160$, $C_d = 0.00000815$, and $u_d = 11600$.

The above results can be viewed in terms of the variation of ϵ_t over incident angles θ as shown in Figure 10. Clearly, with the normal incident speed v fixed, greater tangential elasticity $-\epsilon_t$ is observed at higher incident angles θ, that is, at lower tangential incident speeds u. The discrepancy between the values of ϵ_t determined with Eq. (c') and Eq. (d') appears greater at higher incident angles, signifying that the hard-sphere approximation becomes worse as collisions tend to be more normal. It is also clear from Figure 10 that the tangential elasticity is greater at higher normal incident speeds, indicating the tendency that the tangential and normal elasticities accompany one another.

[3] Model I experiment on Feint glued with PSA To illustrate the use of the present analysis, we perform another Model I experiment on the Butterfly Feint OX long-pips rubbersheet glued to a stationary woodblock with PSA, and compare it with the results from Sriver in [1]. Balls with incident velocities controlled around ($u = 0$ km/h, $v = 30$ km/h) are normally incident on Feint lying in the x-z plane. The incident spin in the z direction is varied from 0 to 200 rps, and the outgoing velocity components (u', v') and spin $n' = \omega'/(2\pi)$ are recorded.

In Figure 11 the normal coefficient of restitution ϵ_n is plotted against the initial spin n, and is compared with the Sriver case. Apparently, ϵ_n is rather uniform over the range of n and falls around 0.605 while Sriver has a greater $\epsilon_n(n = 0) \sim 0.637$ and shows a slight increase as incident spin increases.

For the tangential elasticity, the (n, u') plot is shown in Figure 12a. If the tangential coefficient of restitution were independent of the initial spin and the deformation of colliding members were neglected, the plot would produce a straight line passing through the origin. The best-fit line passing through the origin has a slope $m_1 = 5.2462$ from which the best estimate of ϵ_t can be found: $\epsilon_t(a') = -0.113$ (Figure 12a). Compare this with $\epsilon_t(a') = -0.496$ for Sriver (Figure 12c). A similar procedure applied to the (n, n') plot yields a slope $m_1 = 0.29173$ and the best estimate $\epsilon_t(b') = -0.171$ (Figure 12b), compared with $\epsilon_t(b') = -0.564$ for Sriver (Figure 12d). However, the real behavior of Feint's ϵ_t is far from constant with respect to the initial spin n as shown in Figure 13. At low initial spin up to 20 rps Feint behaves, as expected from an ideal long-pips rubbersheet, as a perfectly slippery surface. However, as n increases from 20 to 70 rps, ϵ_t drops rapidly down to a negative value of ~ -0.1, and appears to stabilize around that value at higher initial spins. This demonstrates that Feint is a complicated rubbersheet which possesss a dual character: At lower relative tangential speeds it exhibits normal (i.e. positive and high in ϵ_t) behavior as a long-pips rubber while at higher relative tangential speeds its character progressively becomes similar to that of typical inverted rubbersheets of low tangential elasticity, or probably that of short pips rubbersheets.

[4] Model I experiment on Sriver glued with trichloroethylene and with But-

terfly Clean Chack Finally, we investigate the effects of trichloroethylene (TCE, Taishin Chemicals Limited) and Butterfly Clean Chack (CC, mainly cyclohexane) on the coefficients of restitution, which we compare with the previous results from PSA. The rubber-sheet used in this experiment is Sriver, and again the Model I procedure is adopted.

Figure 14 reports the variation of ϵ_n over various initial spin velocities when three kinds of adhesives, PSA, TCE, and CC, are used to glue a Sriver rubbersheet on a woodblock. We find that the difference between TCE and CC is not significant while the difference between PSA and the above two is clearly visible: Gluing with special adhesives boosts ϵ_n up to 10% at low relative tangential velocities while the special glue effect becomes less pronounced at higher relative tangential speeds. In other words, gluing with special adhesives helps broaden the range of n over which high ϵ_n is enjoyed by players.

Effects of TCE and CC on ϵ_t can be found by comparing the (n, u') plots and (n, n') plots with those discussed in [1] (Figure 15). In the constant-ϵ_t approximation its best estimate can be obtained from the slope of a line passing through the origin which is best fit to the (n, u') plots: $\epsilon_t(a') = -0.574$ for TCE (Figure 15a) and -0.593 for CC (Figure 15c), compared with -0.496 for PSA (Figure 15e). Thus, a 16% and 20% enhancement of the tangential elasticity is observed by using TCE and CC instead of PSA. This leads us to suspect that special glue effects appear more dramatically in the change of ϵ_t rather than in the change of ϵ_n. The (n, n') plot is not appropriate for the purpose of determining the best estimate of ϵ_t in the constant-ϵ_t approximation, because there is an interval of low n over which the postcollision spin n' nearly vanishes or is reversed in direction. Therefore, we give up the constant-ϵ_t approximation, plot $\epsilon_t(b')$ over a variety of n, and seek its best linear fit. The results are $\epsilon_t(b') = A_1 + B_1 n$ with $A_1 = -0.81627$, $B_1 = 0.0017159$ for TCE, $A_1 = -0.90203$, $B_1 = 0.0030467$ for CC, and $A_1 = -0.81956$, $B_1 = 0.0019609$ for PSA (Figure 16b). The corresponding quadratic approximation to the (n, n') plots yields $n' = C_b n(n - n_b)$ with $C_b = 0.00104$, $n_b = 95.3$ for TCE, $C_b = 0.00184$, $n_b = 81.8$ for CC, and $C_b = 0.00119$, $n_b = 85.0$ for PSA. We suspect that the interval of initial spin n over which the spin reversal occurs, i.e. $0 < n < n_b$ broadens due to the application of TCE or CC. In the quadratic approximation n_b(TCE) shows a 12% increase over n_b(PSA) though n_b(CC) has dropped by 4% . The above nonlinear behavior of $n'(n)$ seems to reflect the effects of TCE and CC to soften the sponge below the rubbersheet to the extent that the incident spin energy is efficiently absorbed and stored as strain energy of the rubber-sponge complex. In fact, the experimental results in Figure 15b, 15d, and 15f show more clearly that the range of n which gives rise to almost vanishing n' is 38 rps $< n <$ 150 rps for TCE, 19 rps $< n <$ 98 rps for CC, and 34 rps $< n <$ 110 rps for PSA, signifying the obvious advantage of TCE over CC or PSA. Finally, the values of ϵ_t obtained from Eq. (a') are plotted against n for the three kinds of adhesives in Figure 16a. Just as seen in Figure 14 for ϵ_n there are obvious enhancements in tangential elasticity at low initial spins. The enhancement factor reaches almost 200% for CC at extremely low n while it tends to diminish to 100% (no enhancement) as n approaches 150 rps.

However, the above results are only preliminary and must be viewed with some caveats since there are many important experimental factors to be carefully controlled, including the initial concentration of the adhesives, and the time dependence of their concentration, i.e. the speed of volatile loss in the rubber-sponge complex. The authors believe that this

line of research will have a capability of providing players as well as manufacturers in our sport with much beneficial and quantitative information.

8. CONCLUSION

In the present investigation we have examined the collisional interactions of the table tennis balls with two types of rubber glued to a woodblock with a choice of adhesives in terms of two significant parameters, the normal coefficient of restitution ϵ_n and the tangential coefficient of restitution ϵ_t, under the major assumption of hard-sphere collisions. Our main results and conclusions have been stated in Section **7.** Research along this line has only begun. We have confirmed that neither coefficient of restitution is generally independent of the incident relative velocity. Thus, unfortunately a simple description of collision dynamics in terms of constant coefficients of restitution turns out to be insufficient to account for the complex ball-racket interactions. Still, it has been demonstrated that by allowing for the velocity dependence of these coefficients and by keeping the limitations of the hard-sphere models in mind, a wealth of significant information can be uncovered as a result of experimental and theoretical methods presented in this paper. Extension to the present work includes the investigation of a more complete variety of rubbersheets, sponge quality and thickness, blade quality and thickness, adhesive composition and concentration over a more extensive and continuous range of incident parameters. Most importantly, however, models of collisional deformation must be incorporated while retaining as much simplicity of hard-sphere collisions as possible.

ACKNOWLEDGMENTS

The present experimental research was conducted at the Tokorozawa Laboratory of Tamasu Company Limited, Japan between July 1994 and April 1995 by S. Sato and H. Yamazaki. Data analysis and theoretical calculation were performed by S. Araki and H. Yamazaki. S. Araki gratefully acknowledges an extremely generous research support granted by Kimihiko Tamasu, President, and Hikosuke Tamasu, Chairman of Tamasu Company Limited, for his visits to Tokorozawa Laboratory in July 1994 and in May 1995, and for his participation in the 4th ITTF Sports Science Congress in Beijing, China in April 1995.

The Hofstra University Faculty Travel Fund is also gratefully acknowledged for its partial support of his participation in the above conference.

S. Araki extends his special thanks to Goro Shibutani of Tamasu for exceptionally thoughtful arrangements in order to make his research visits fruitful. He could not thank Shotaro Kubo and Fumio Terano, both of Tamasu, too much for their warmest hospitality, far more than he deserved, during his second visit to Tamasu in May 1995. He thanks Hisashi Kubo of Chuo University and Kady Choy of Hofstra University for their assistance in data analysis.

The authors cordially thank Rufford Harrison of ITTF, Yutaka Tsuji of Osaka University, and Fujio Yamamoto of Fukui University for their time and trouble in reviewing the manuscript. A detailed and enthusiastic review by Harrison has significantly improved

its quality.

Finally, S. Araki would like to dedicate this paper to the late ITTF President, Ichiro Ogimura. May he rest in peace and enjoy observing the steady growth of the Academy he founded.

REFERENCES

Araki, S. (1988). The dynamics of particle disks II. Effects of spin degrees of freedom. *Icarus* **76** 182–198.

Araki, S. (1991a). The dynamics of particle disks III. Dense and spinning particle disks. *Icarus* **90** 139–171.

Araki, S. (1991b). Dynamics of planetary rings. *American Scientist* **79** 44–59.

Araki, S., and Tremaine, S. (1986). The dynamics of dense particle disks. *Icarus* **65** 83–109.

Bridges, F. G., Hatzes, A. P., and Lin, D. N. C. (1984). Structure, stability, and evolution of Saturn's rings. *Nature* **309** 333–335.

Hatzes, A. P., Bridges, F. G., and Lin, D. N. C. (1988). Collisional properties of ice spheres at low impact velocities. *M. N. R. A. S.* **231** 1091–1115.

Hatzes, A. P., Bridges, F. G., Lin, D. N. C., and Sachtjen, S. (1991). Coagulation of particles in Saturn's rings: Measurements of the cohesive forces of water frost. *Icarus* **89** 113–121.

International Table Tennis Federation (1995). Handbook 1995–1997. Ed. Williams, E. *The International Table Tennis Federation* **26th Edition**, 2.1.3.

Kawazoe, Y. (1992). Ball/racket impact and computer aided design of rackets. *Intl. J. T. T. Sci.* **1** 9–18.

Savage, S. B., and Sayed, M. (1984). Stress developed by dry cohesionless granular materials sheared in an annular shear cell. *J. Fluid Mech.* **142**, 391–430.

Supulver, K. D., Bridges, F. G., and Lin, D. N. C. (1995). The coefficient of restitution of ice particles in glancing collisions: Experimental results for unfrosted surfaces. *Icarus* **113** 188–199.

Tiefenbacher, K., and Durey, A. (1994a). The impact of the table tennis ball on the racket. *ITTF Table Tennis Digest* **17** 3–11.

Tiefenbacher, K., and Durey, A. (1994b). The impact of the table tennis ball on the racket

(Backside coverings). *Intl. J. T. T. Sci.* 2 1–14.

Wu, H. Q., Qin, Z. F., Xu, S. F., and Xi, E. T. (1992). Experimental research in table tennis spin. *Intl. J. T. T. Sci.* 1 73–78.

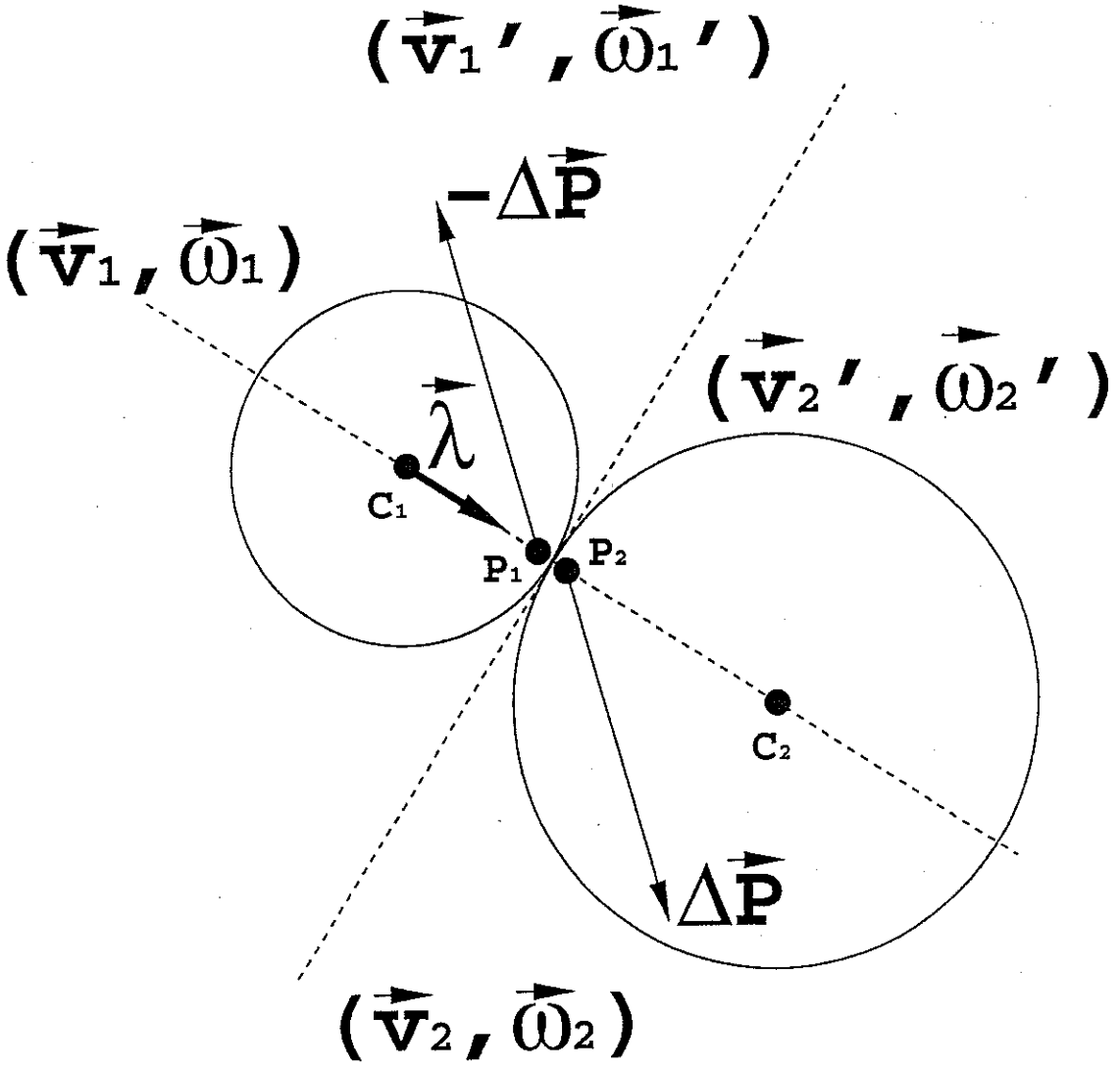

Figure 1 A schematic diagram of a two-body hard-sphere collision in three dimensions. A hard-sphere particle is fully characterized by its mass, radius, and moment of inertia. Particle i with initial linear and angular velocities $\vec{v}_i$ and $\vec{\omega}_i$ undergoes a collision and ends up with final velocities $\vec{v}_i'$ and $\vec{\omega}_i'$, where $i = 1, 2$. At the instant of the collision the center of Particle i is located at Point C_i, and Particle 1 exerts an impulse $\vec{\Delta}P$ on Particle 2 at Point P_2 while Particle 2 exerts a reaction impulse $-\vec{\Delta}P$ on Particle 1 at Point P_1.

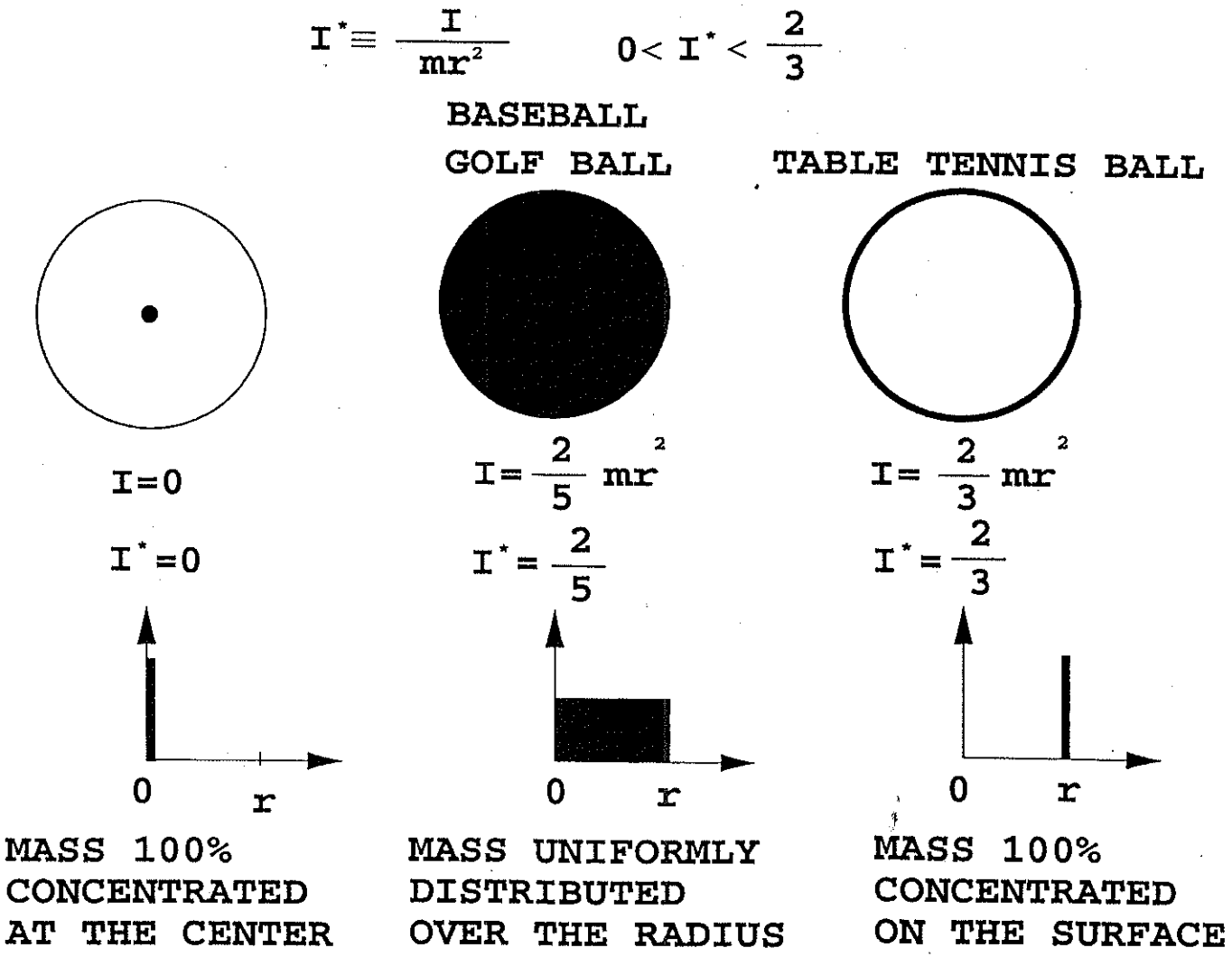

Figure 2 The definition of the dimensionless moment of inertia, $I^* = I/(mr^2)$, and its range. Its minimum value $I^* = 0$ corresponds to a sphere whose mass is all concentrated at its center while the maximum value $I^* = 2/3$ is attained for a sphere whose total mass is concentrated on its surface.

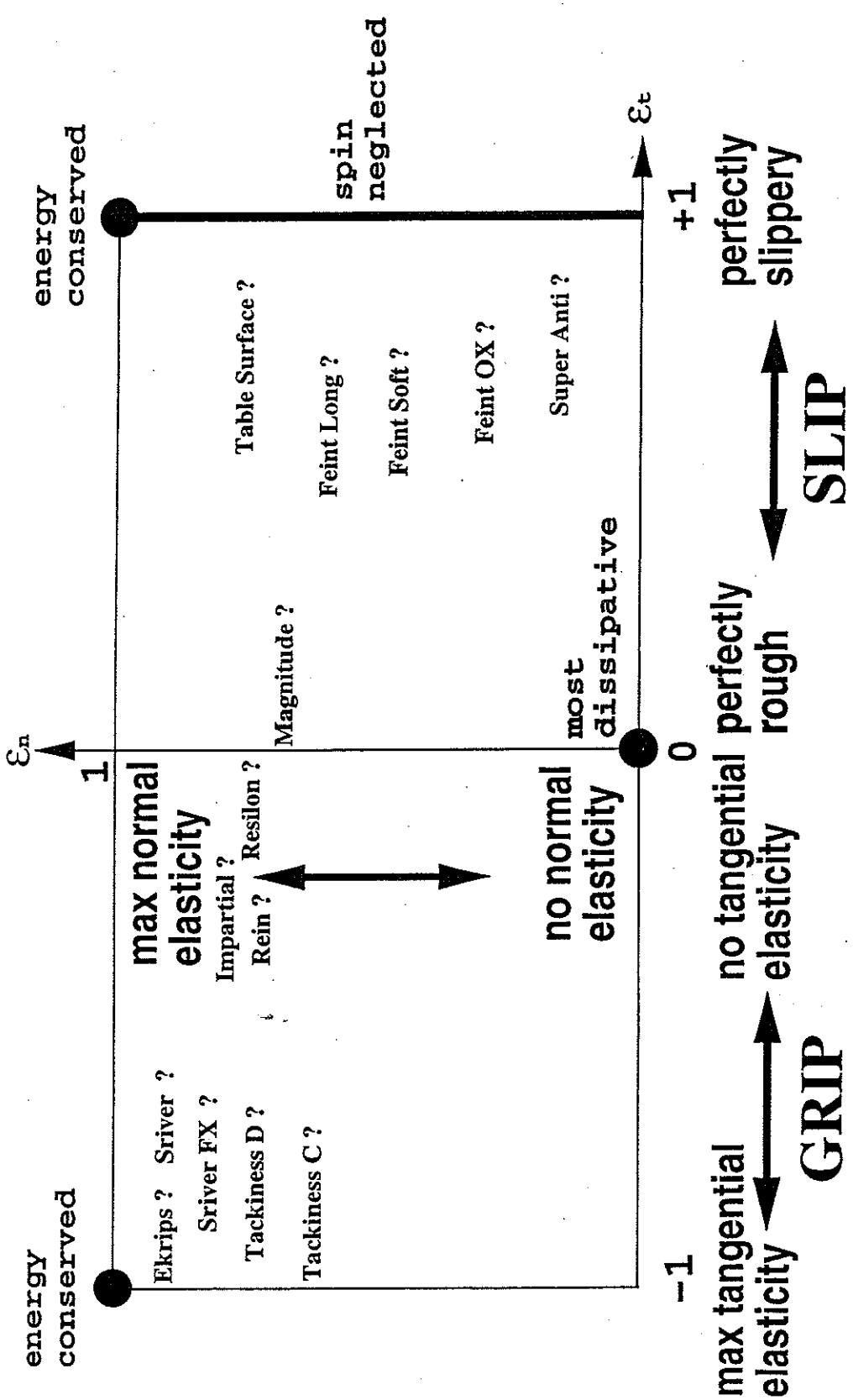

Figure 3 The parameter space spanned by the normal and tangential coefficients of restitution (ϵ_t, ϵ_n) showing the comprehensive coverage of surface properties of table tennis rubbersheets and table surfaces when the balls collide with them. Best estimates, based on our experience, of the average surface properties of the popular rubbersheets manufactured by Tamasu as of April 1995 are indicated in this parameter space. Note that these estimates do not result from the current research.

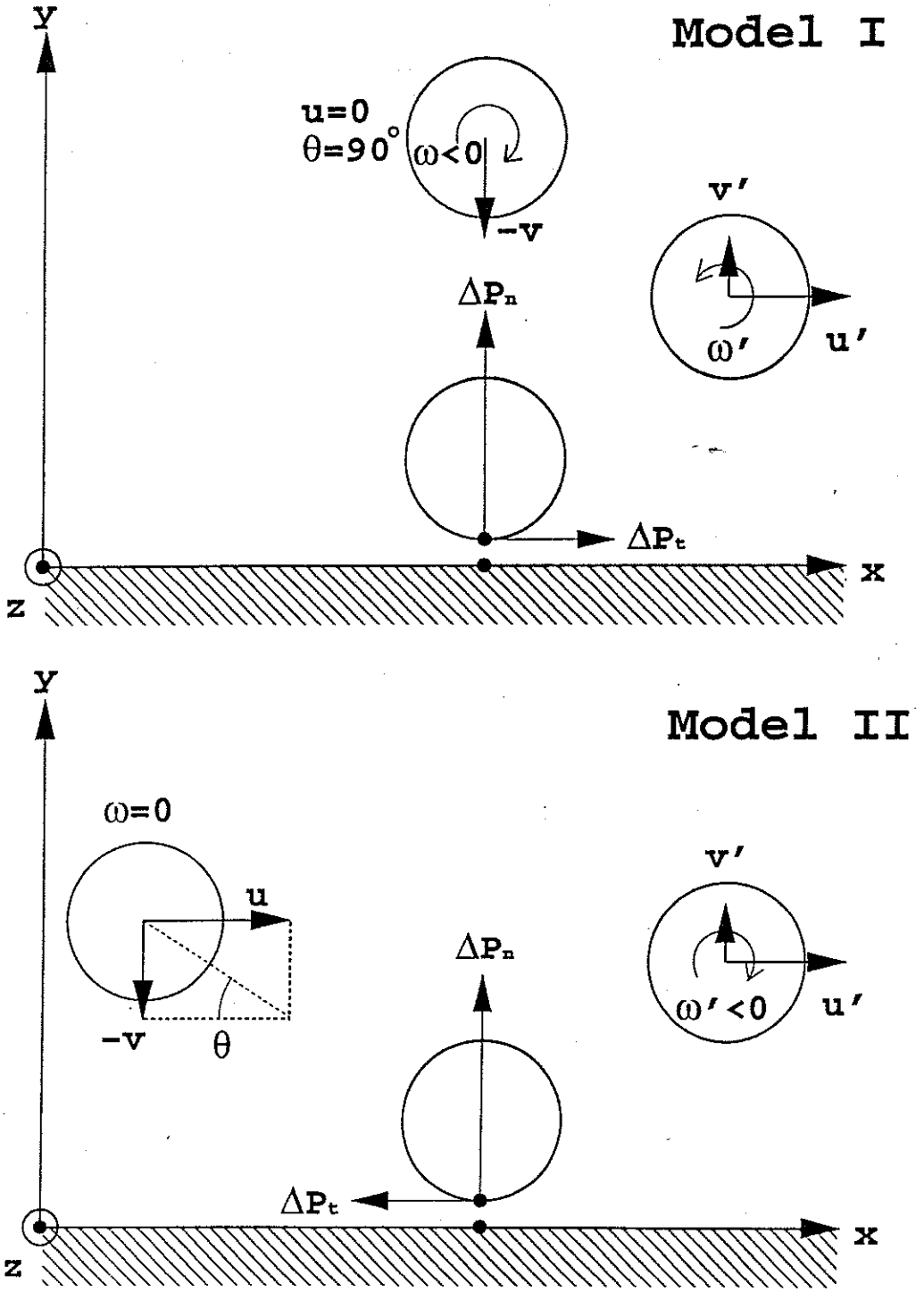

Figure 4 A schematic diagram of Model I and Model II experiments. In both experiments the racket surface lies in the x-z plane and the two dimensional collision event is confined within the x-y plane. In Model I experiments balls are released vertically downward with a given initial speed v and with different clockwise initial spins ω. In Model II experiments balls without spin and with a given vertical speed are shot at various horizontal incident speeds u. i.e. at various incident angles θ.

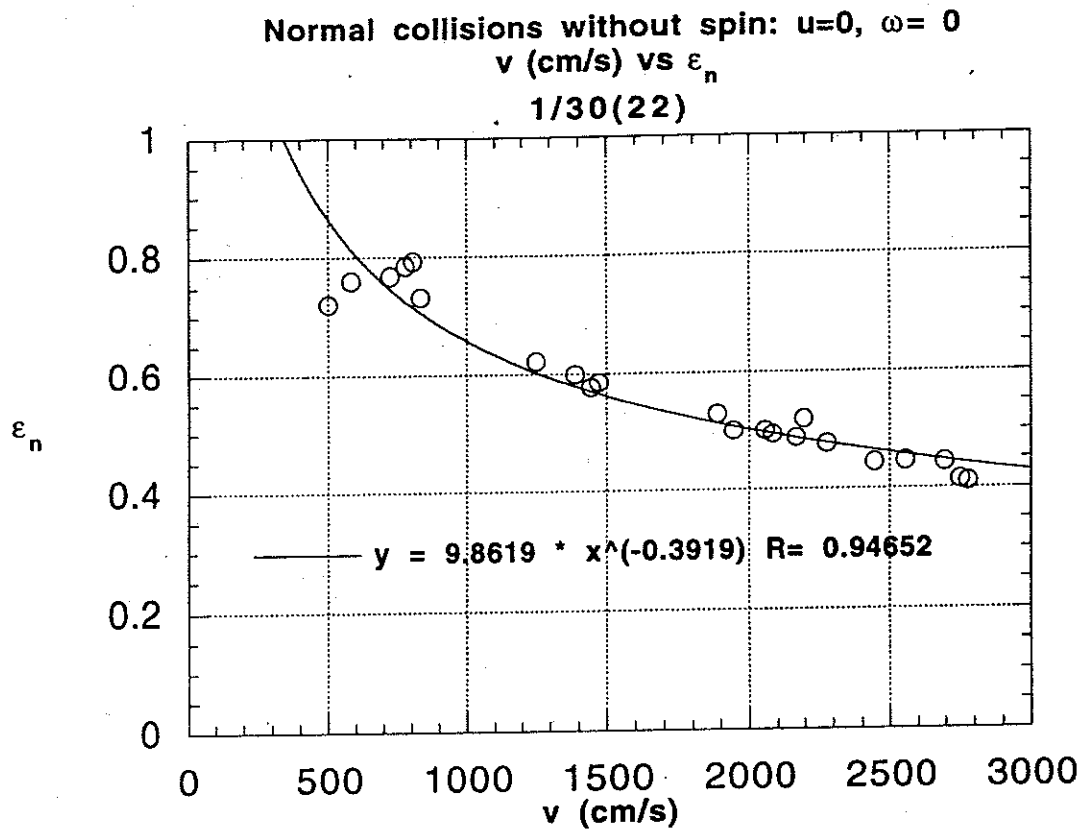

Figure 5 The velocity dependence of the normal coefficient of restitution. Balls without spin are shot normal to the Sriver rubbersheet glued to a woodblock with PSA. Incident normal velocities are in cm/s. The best power-law fit and corresponding equation are displayed.

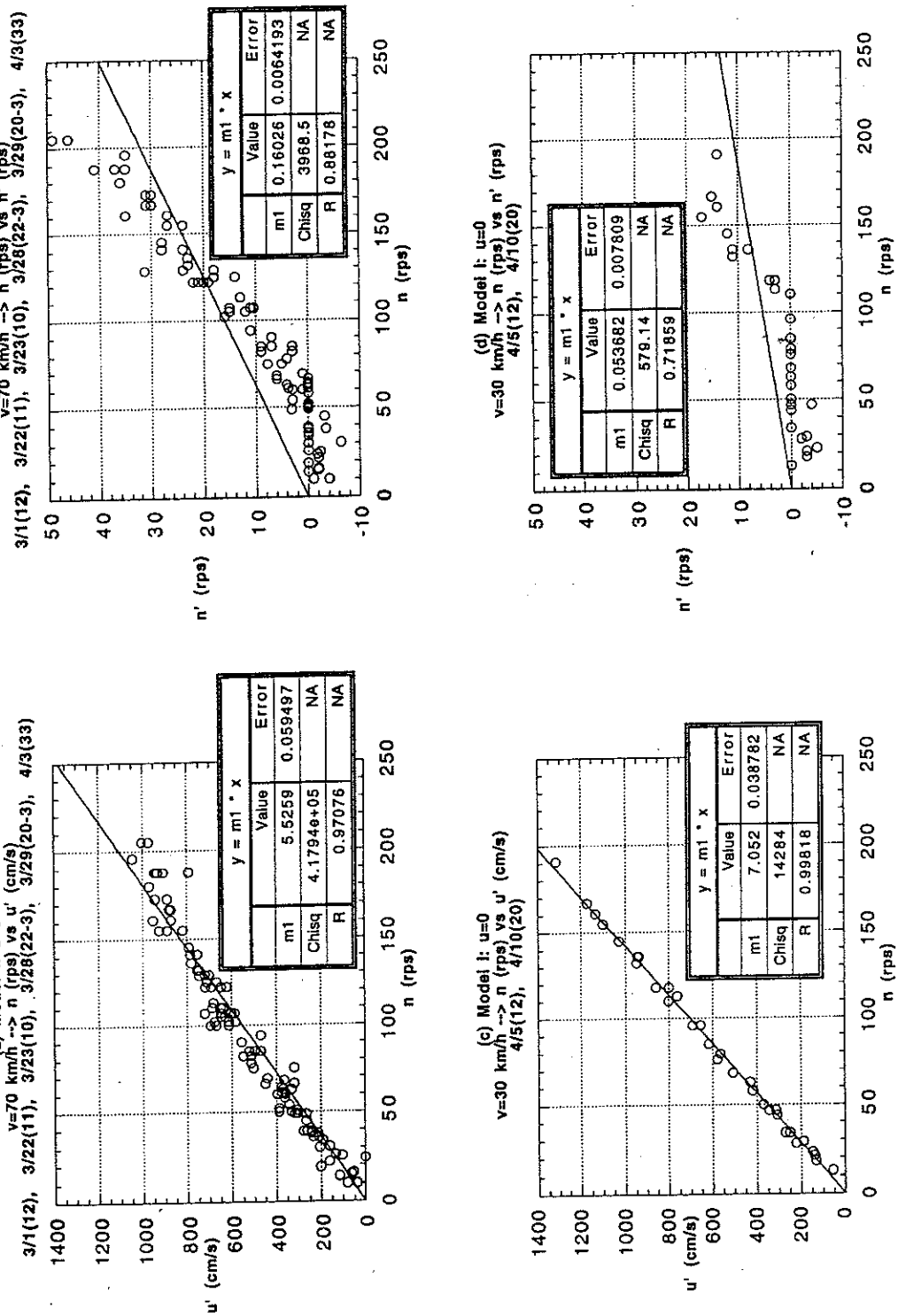

Figure 6 Model I experiments on collisions of the balls with a basic Sriver red rubbersheet on 1.9 mm-sponge glued to a woodblock with PSA. Incident and outgoing spins are in revolutions per second (rps) while the tangential component u' of the outgoing velocities is in cm/s. (a) (n, u') with incident normal speed $v = 70$ km/h. (b) (n, n') with incident normal speed $v = 70$ km/h. (c) (n, u') with incident normal speed

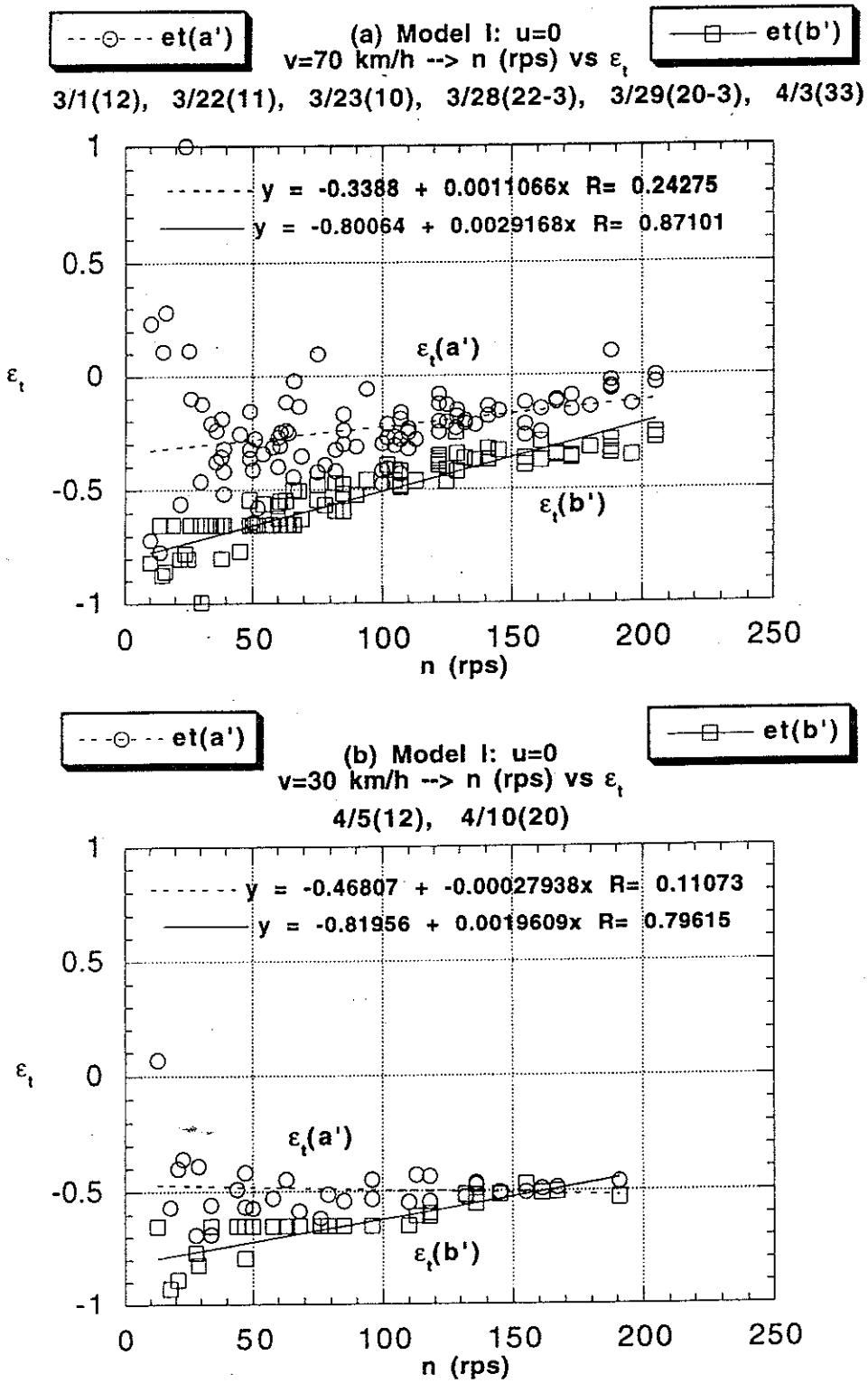

Figure 7 Model I experiments on collisions of the balls with a basic Sriver red rubbersheet on 1.9 mm-sponge glued to a woodblock with PSA. Incident spin n is in revolutions per second (rps). (a) (n, ϵ_t) with incident normal speed $v = 70$ km/h. (b) (n, ϵ_t) with incident normal speed $v = 30$ km/h. A data set with circular symbols is generated with the use of Eq. (a') while another data set with square symbols is obtained with the use of Eq. (b'). The best linear fits and corresponding equations are displayed.

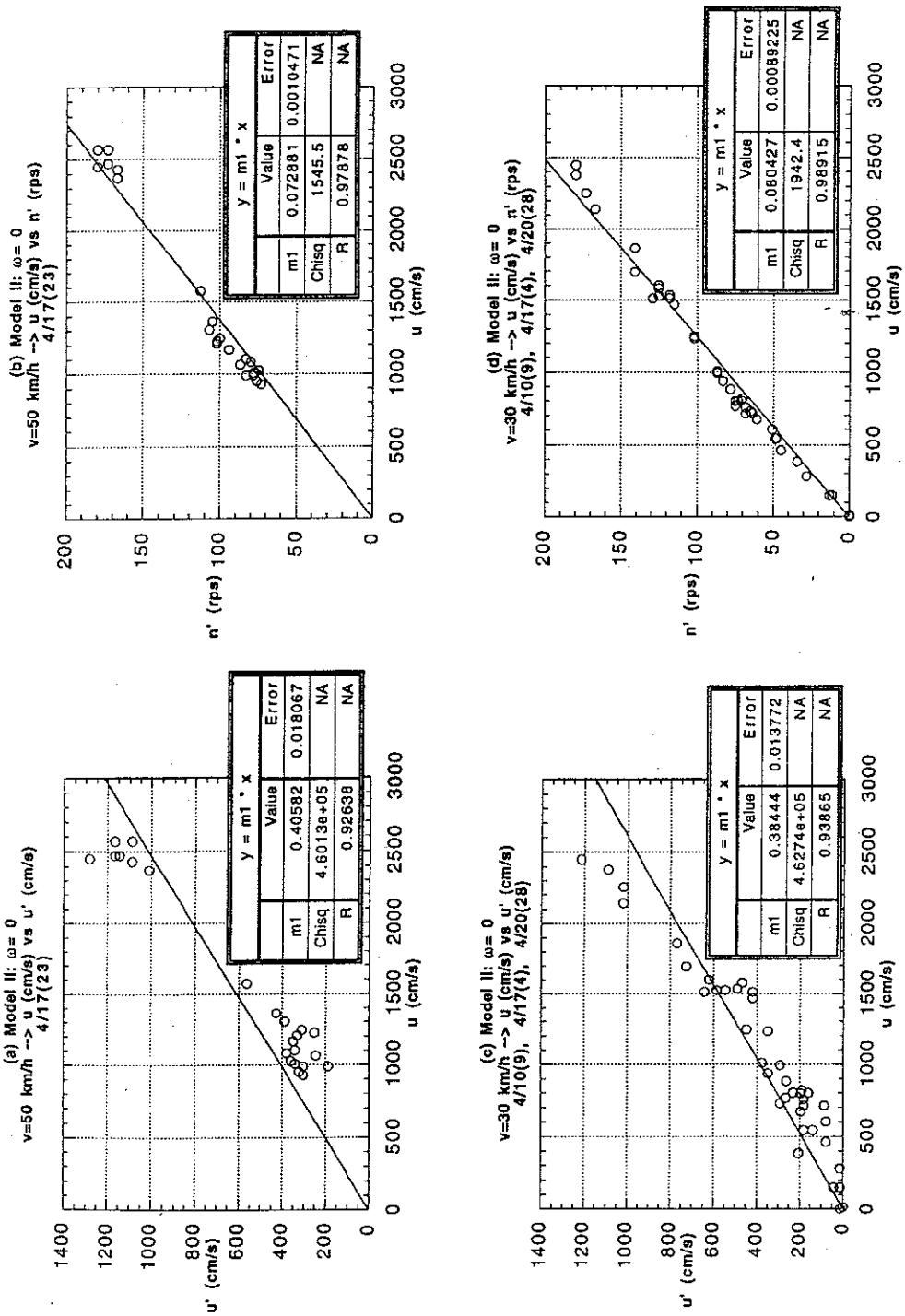

Figure 8 Model II experiments on collisions of the balls with a basic Sriver red rubbersheet on 1.9 mm-sponge glued to a woodblock with PSA. Outgoing spin n' is in revolutions per second (rps) while the tangential components u and u' of the incident and outgoing velocities are in cm/s. (a) (u, u') with incident normal speed $v = 50$ km/h. (b) (u, n') with incident normal speed $v = 50$ km/h. (c) (u, u') with incident normal speed $v = 30$ km/h. (d) (u, n') with incident normal speed $v = 30$ km/h. The best linear fit passing through the origin to each plot yields an estimate of ϵ_t if it is assumed constant.

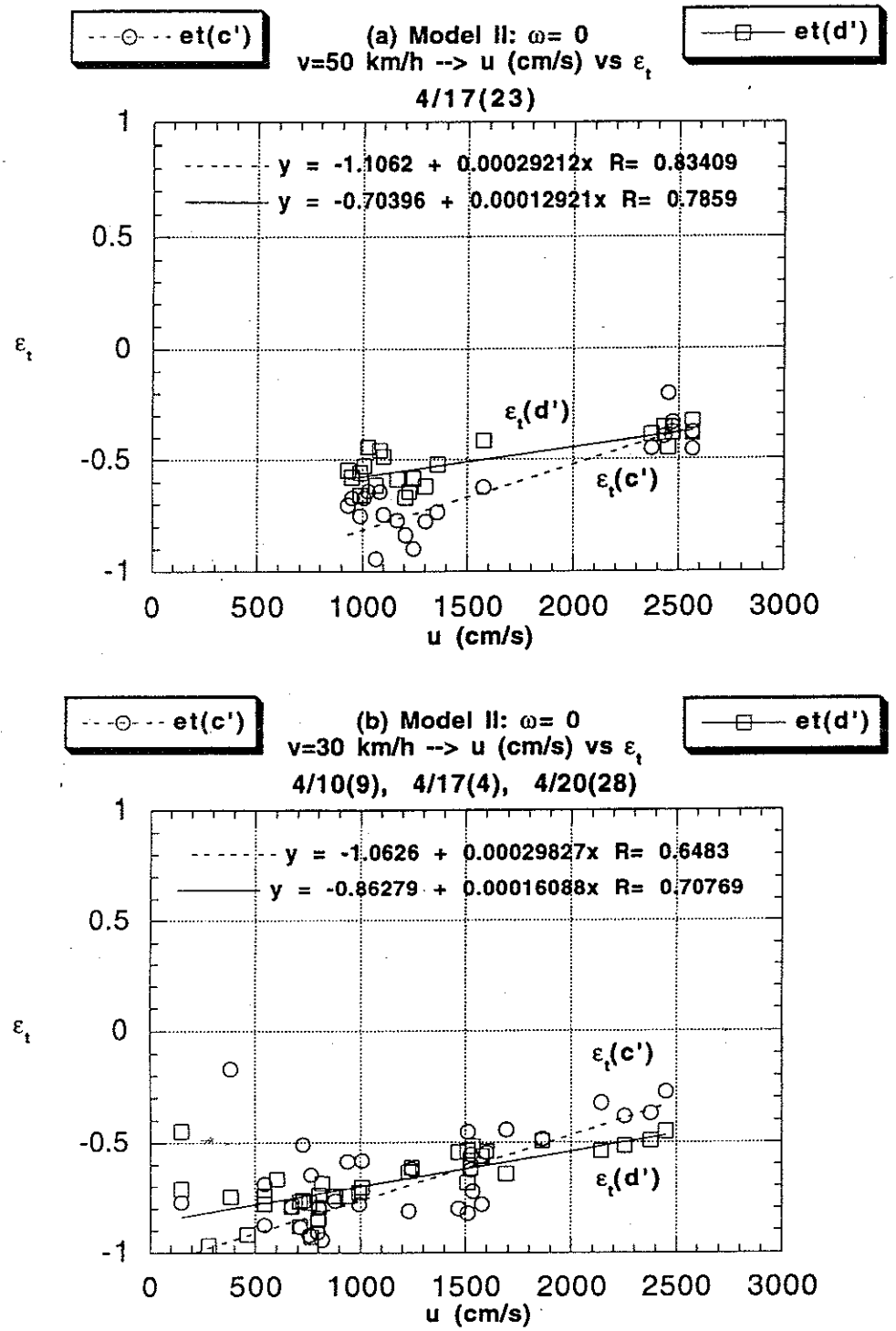

Figure 9 Model II experiments on collisions of the balls with a basic Sriver red rubbersheet on 1.9 mm-sponge glued to a woodblock with PSA. Incident tangential speed u is in cm/s. (a) (u, ϵ_t) plot with incident normal speed $v = 50$ km/h. (b) (u, ϵ_t) plot with incident normal speed $v = 30$ km/h. A data set with circular symbols is generated with the use of Eq. (c') while another data set with square symbols with the use of Eq. (d'). The best linear fits and corresponding equations are displayed.

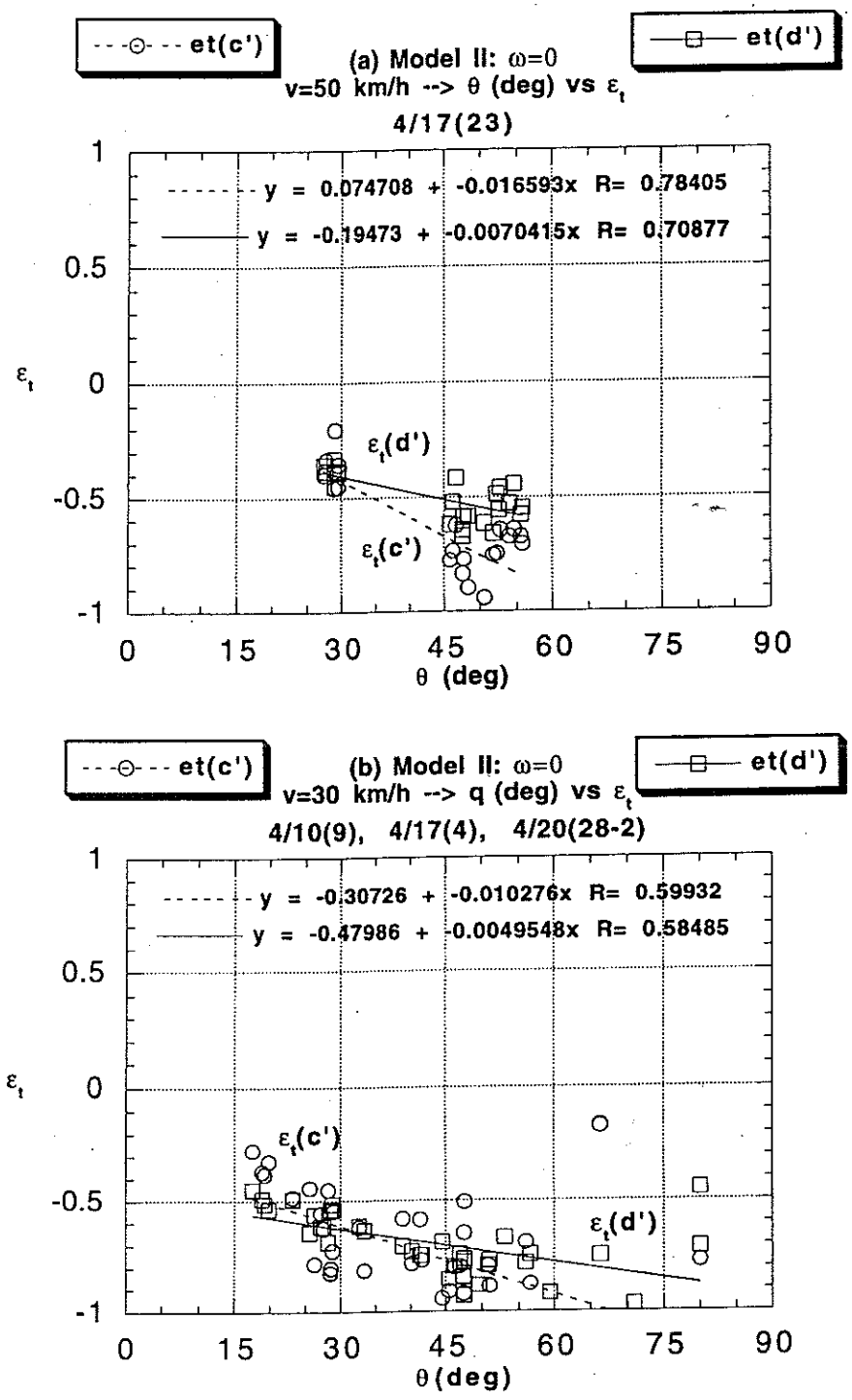

Figure 10 Model II experiments on collisions of the balls with a basic Sriver red rubbersheet on 1.9 mm-sponge glued to a woodblock with PSA. The incident angle θ with respect to the racket surface is in degrees. (a) (θ, ϵ_t) with incident normal speed v = 50 km/h. (b) (θ, ϵ_t) with incident normal speed v = 30 km/h. A data set with circular symbols is generated with the use of Eq. (c') while another data set with square symbols is obtained with the use of Eq. (d'). The best linear fits and corresponding equations are displayed.

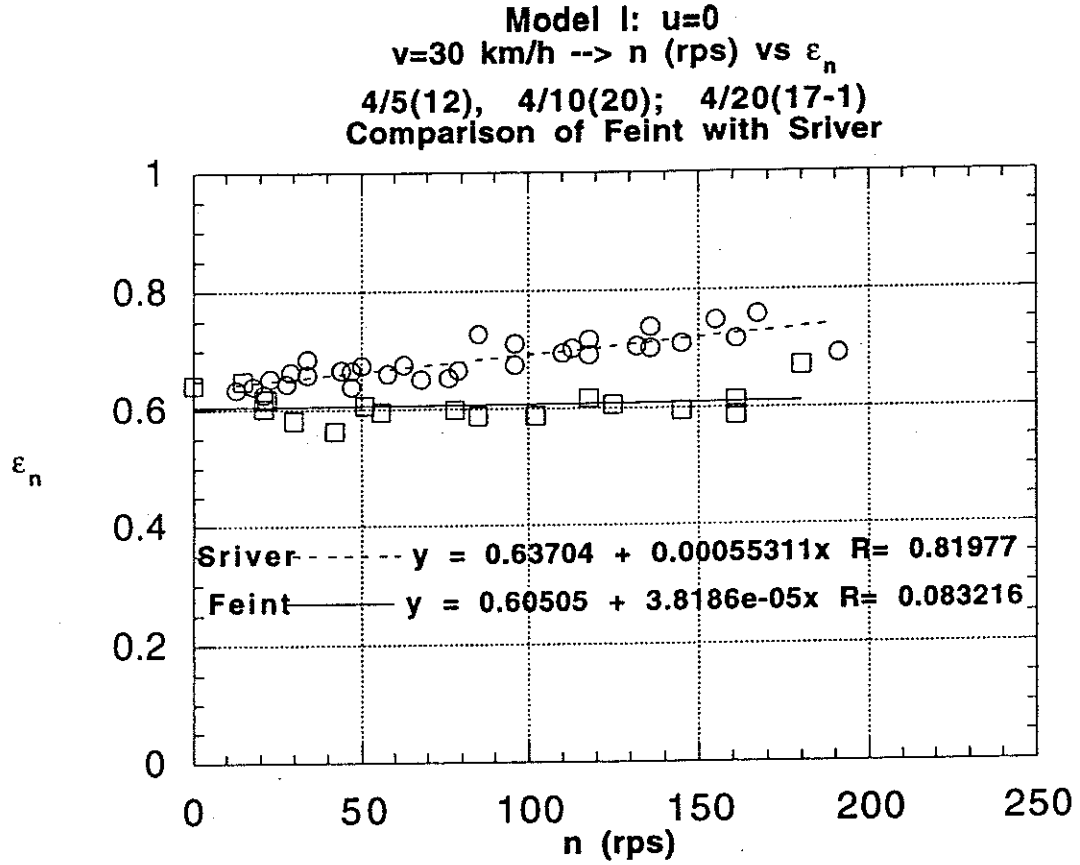

Figure 11 Comparison of Feint OX with Sriver on 1.9 mm-sponge by Model I experiments. $(n,\ \epsilon_n)$ plot with incident normal speed $v = 30$ km/h. Circular symbols represent the data for Sriver while square symbols represent those for Feint OX. Both rubbersheets are glued to a woodblock with PSA. The best linear fits and corresponding equations are displayed. Apparently, ϵ_n is rather insensitive to the initial spin n.

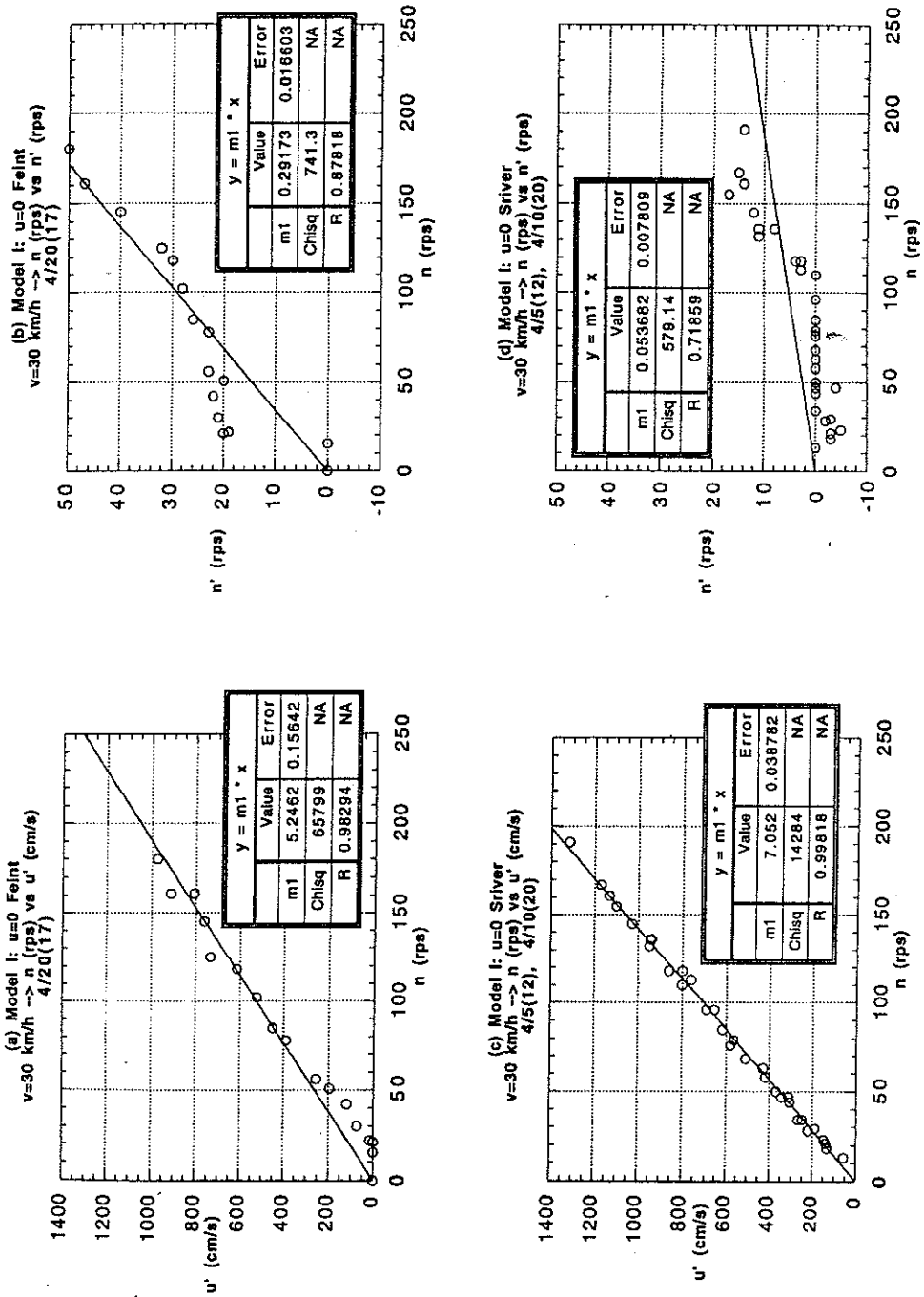

Figure 12 Model I experiments on collisions of the balls with a Feint OX rubbersheet glued to a woodblock with PSA. Incident and outgoing spins are in revolutions per second (rps) while the tangential component u' of the outgoing velocities is in cm/s. Incident normal speed is set to $v = 30$ km/h. (a) (n, u') for Feint OX. (b) (n, n') for

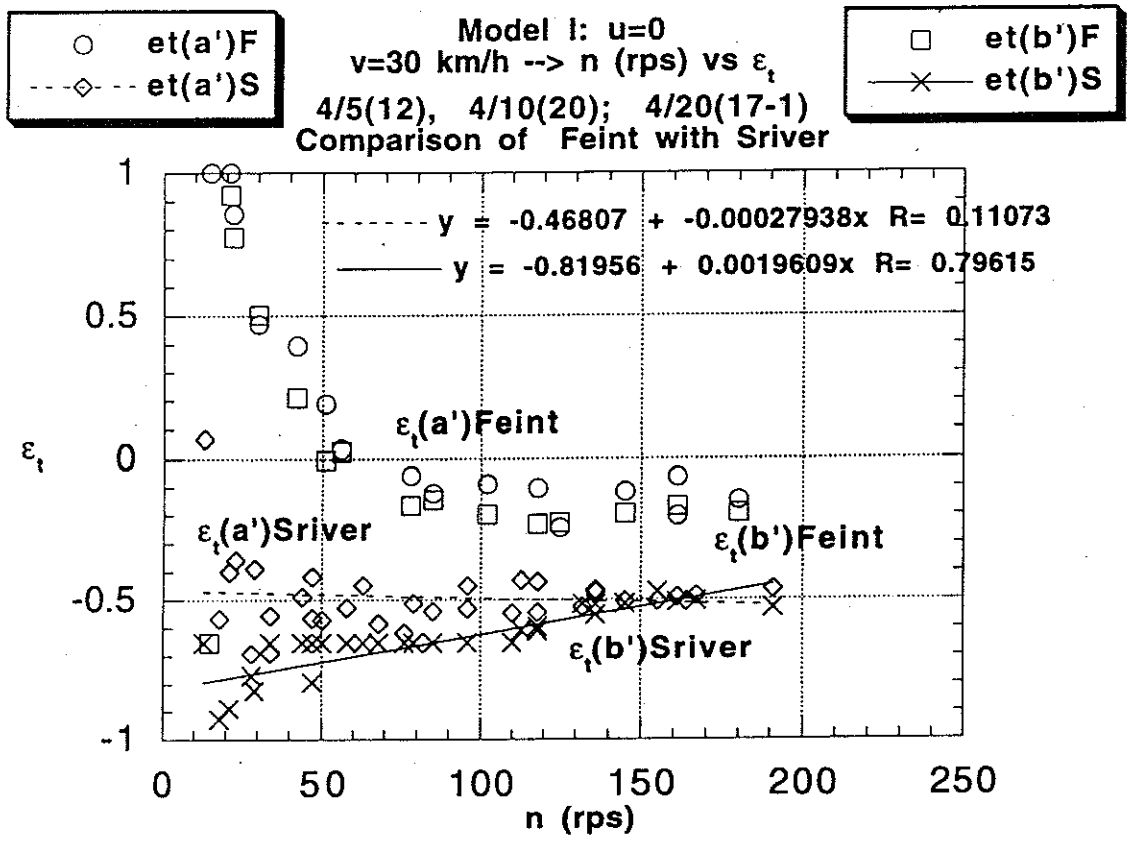

Figure 13 Comparison of Feint OX with Sriver on 1.9 mm-sponge. Model I experiments on collisions of the balls with Feint and with Sriver to determine the dependence of ϵ_t on the initial spin n. Both rubbersheets are glued to a woodblock with PSA. Incident normal speed is set to $v = 30$ km/h. Incident spin n is in revolutions per second (rps). Circular and square symbols represent the (n, ϵ_t) data sets for Feint obtained with the use of Eq. (a') and Eq. (b'), respectively. Diamond and cross symbols represent the (n, ϵ_t) data sets for Sriver obtained with the use of Eq. (a') and Eq. (b'), respectively. The best linear fits and corresponding equations are displayed.

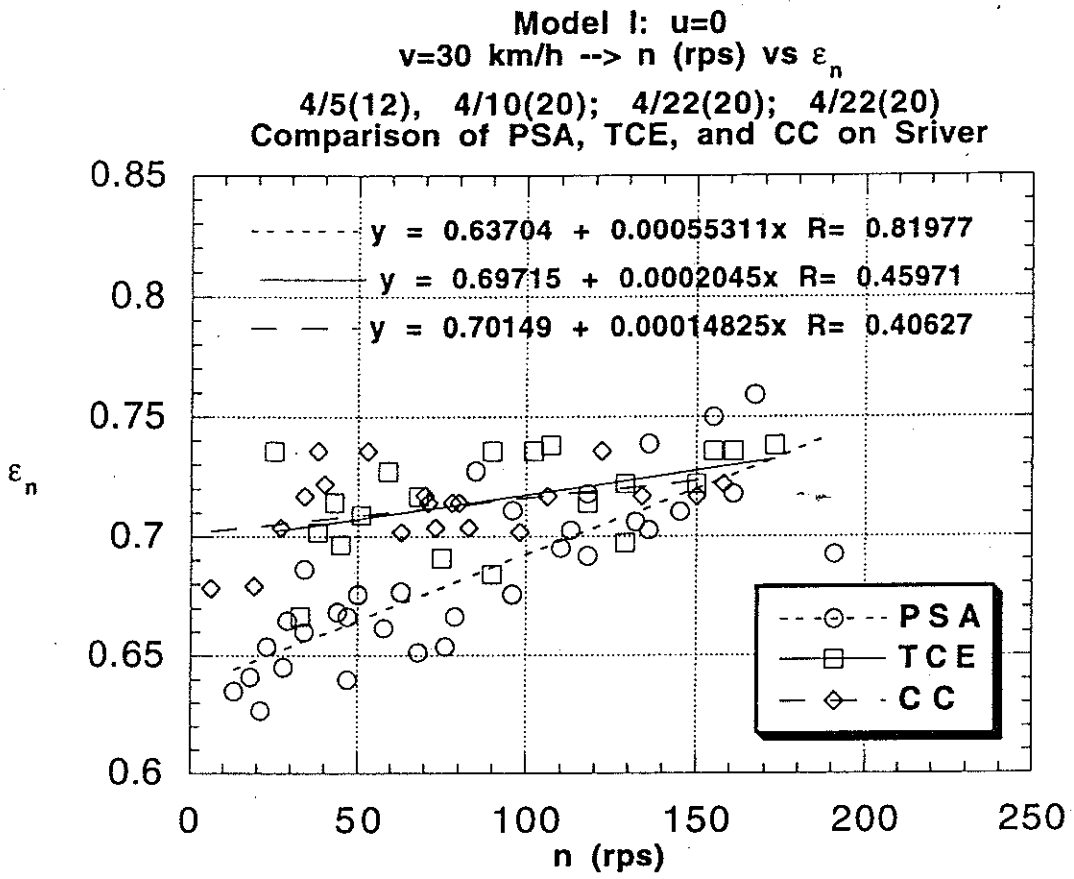

Figure 14 Comparison of PSA, TCE, and Clean Chack applied to Sriver on 1.9 mm-sponge. The dependence of ϵ_n on the initial spin n is determined for each adhesive by Model I experiments. The initial normal speed is set to $v = 30$ km/h. Circular, square, and diamond symbols represent the data with PSA, TCE, and Clean Chack, respectively. The best linear fits and corresponding equations are displayed.

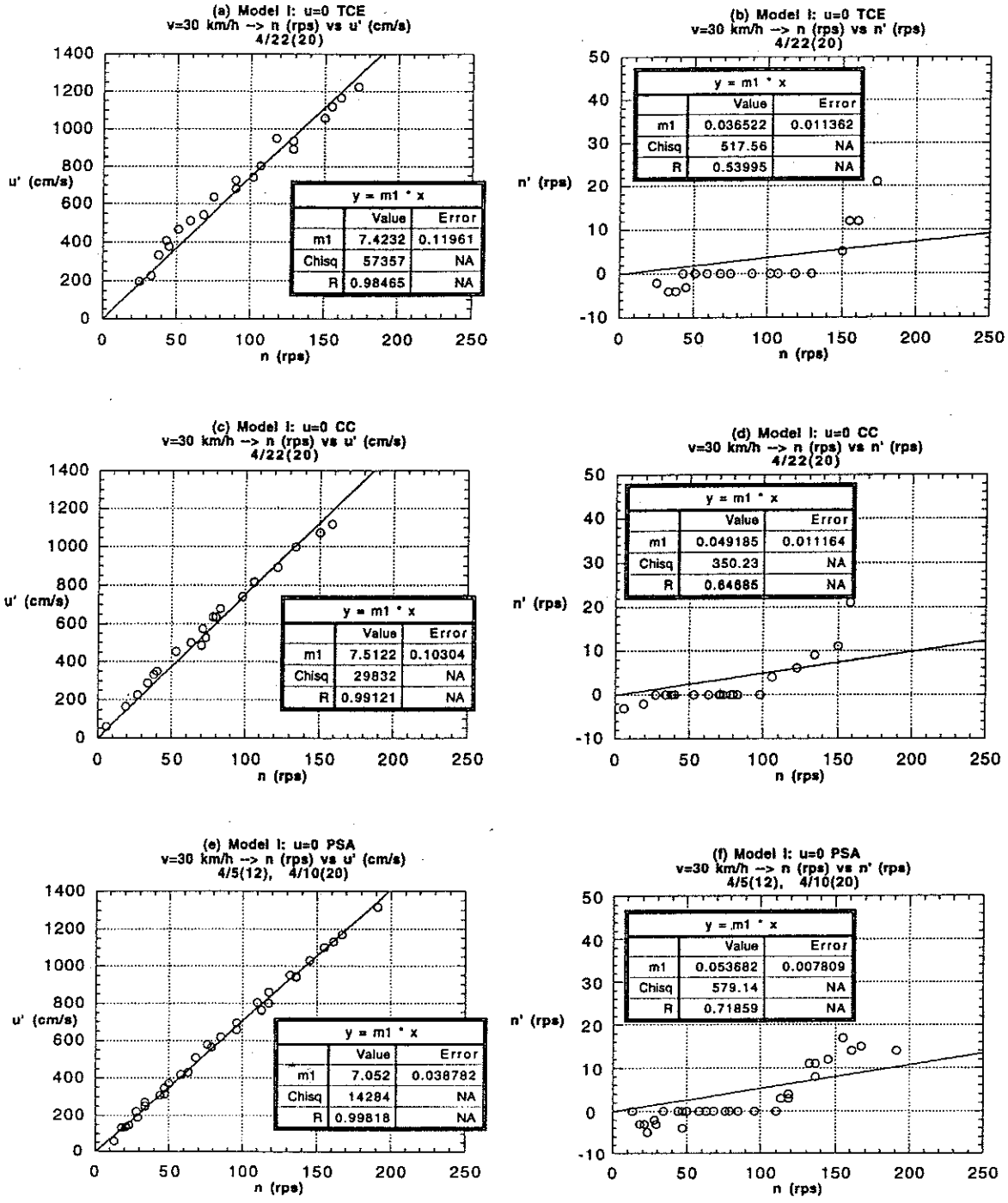

Figure 15 Model I experiments on collisions of the balls with a basic Sriver rubbersheet on 1.9 mm-sponge glued to a woodblock with TCE, with Clean Chack, and with PSA. Incident and outgoing spins are in revolutions per second (rps) while the tangential component u' of the outgoing velocities is in cm/s. Incident normal speed is set to $v = 30$ km/h. (a) (n, u') with TCE. (b) (n, n') with TCE. (c) (n, u') with CC. (d) (n, n') with CC. (e) (n, u') with PSA. (f) (n, n') with PSA. The best linear fit passing through the origin to each plot yields an estimate of ϵ_t if it is assumed constant.

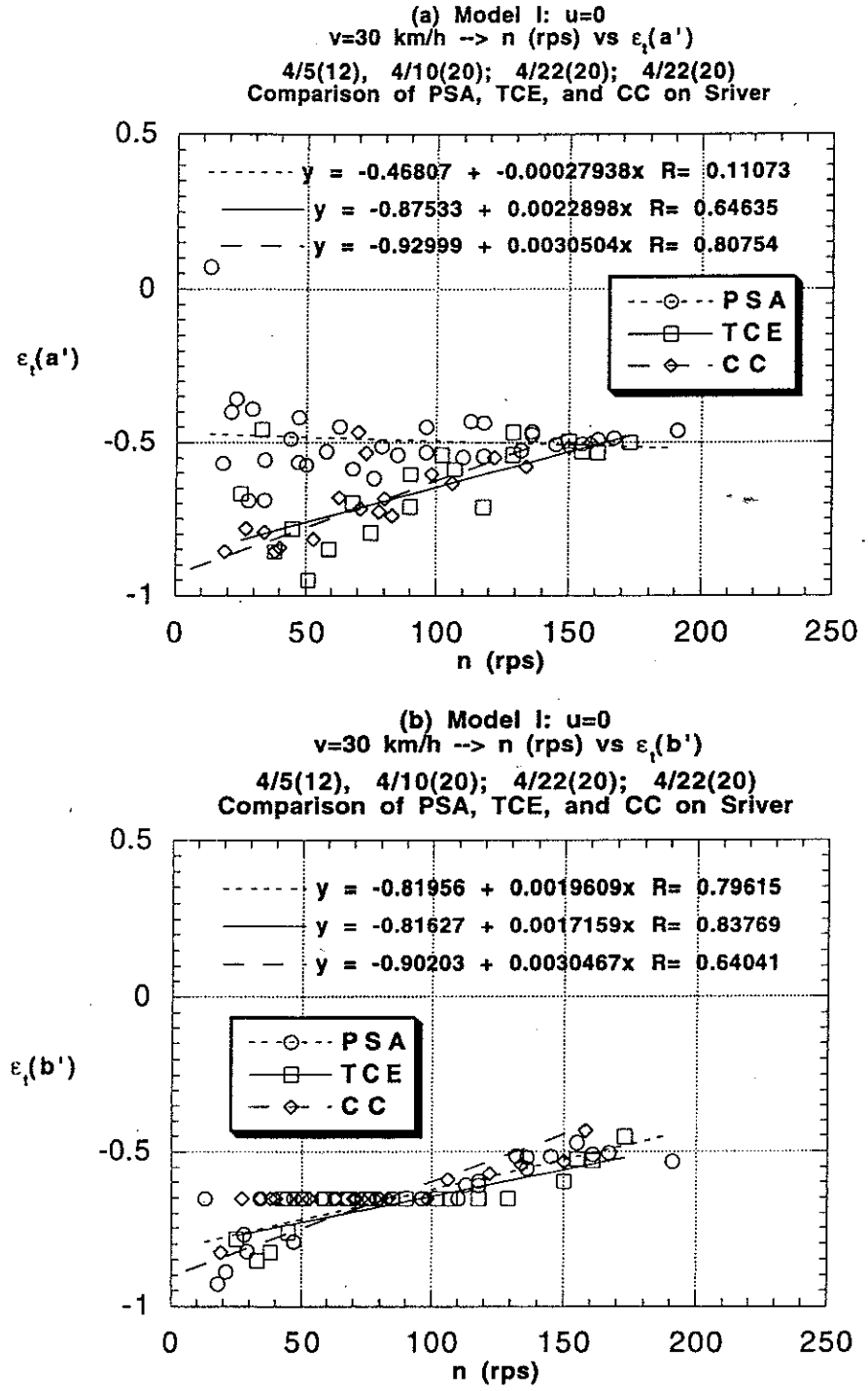

Figure 16 Comparison of PSA, TCE, and Clean Chack applied to Sriver on 1.9 mm-sponge. The dependence of ϵ_t on the initial spin n is determined for each adhesive by Model I experiments. The initial normal speed is set to $v = 30$ km/h. (a) Circular, square, and diamond symbols represent the data obtained with the use of Eq. (a') for PSA, TCE, and Clean Chack, respectively. (b) Circular, square, and diamond symbols represent the data obtained with the use of Eq. (b') for PSA, TCE, and Clean Chack, respectively. The best linear fits and corresponding equations are displayed.